Development of a Three-Axis Inductive Force Sensor for Measuring Tool-Tissue Forces in Robotic Surgery

Author

Muhammad Abdullah Khalid

00000317706

Supervised by

Dr. Muhammad Mubasher Saleem

MASTERS IN MECHATRONICS ENGINEERING,

DEPARTMENT OF MECHATRONICS ENGINEERING

COLLEGE OF ELECTRICAL & MECHANICAL ENGINEERING

NATIONAL UNIVERSITY OF SCIENCES AND TECHNOLOGY,

ISLAMABAD, PAKISTAN

Aug 2022

Development of a Three-Axis Inductive Force Sensor for Measuring Tool-Tissue Forces in Robotic Surgery

Author

Muhammad Abdullah Khalid

00000317706

A thesis submitted in partial fulfillment of the requirements for the degree of MS Mechatronics Engineering

Supervised by

Dr. Muhammad Mubasher Saleem

Thesis Supervisor's Signature:

_____

MASTERS IN MECHATRONICS ENGINEERING,

DEPARTMENT OF MECHATRONICS ENGINEERING

COLLEGE OF ELECTRICAL & MECHANICAL ENGINEERING

NATIONAL UNIVERSITY OF SCIENCES AND TECHNOLOGY,

ISLAMABAD, PAKISTAN

Aug 2022

Declaration

I certify that this research work titled "*Development of a Three-Axis Inductive Force Sensor for Measuring Tool-Tissue Forces in Robotic Surgery"* is my work. It has not been presented elsewhere for assessment. The material that has been used from other sources has been properly acknowledged/referred.

Signature of Student

Muhammad Abdullah Khalid

00000317706

Language Correctness Certificate

This thesis has been read by an English expert and is free of typing, syntax, semantic, grammatical and spelling mistakes. The thesis is also according to the format given by the university.

Signature of Student

Muhammad Abdullah Khalid

00000317706

Signature of Supervisor

Copyright Statement

Acknowledgments

I am utmost grateful to Almighty Allah, the most powerful and merciful. He has always guided me to the right objectives in life. After the Lord, I am thankful to my parents for their consistent motivation and support in accomplishing goals throughout my life while remaining optimistic.

I heartily appreciate the efforts of my master's supervisor, Dr. Muhammad Mubasher Saleem, Associate Professor and Associate Head of the Department of Mechatronics Engineering, College of E&ME, NUST. I am thankful for his mentorship in developing my interest in a research field. His incredible devotion in this project's research and development phase has made it possible to complete the project timely. I have benefited from his guidance during the work, which kept me on track while learning the research process, increasing my knowledge, and polishing my skills.

I am thankful to my GEC members, Dr. Mohsin Islam Tiwana and Dr. Amir Hamza, for their time and guidance in this research.

Finally, I thank my colleagues and seniors in the project lab who inspired me and supported me in the project.

Dedicated to my exceptional parents and loving siblings whose tremendous support and cooperation led me to this wonderful accomplishment

Abstract

Robotic surgeries are becoming popular because of their benefits over traditional procedures. In robot-assisted surgery, surgeons cannot judge the amount of force the tools exert on a patient's tissues and sensitive internal body parts. This lack of force feedback has been reported to cause damage to healthy tissue and post-surgery complexities. This problem has two parts: one requires building a force sensor to precisely estimate the amount of force applied to the patient during surgery. The other part consists of making an actuator to transfer or define the amount of force to surgeons. This work has proposed a three-axis tactile force sensor that can be integrated with modern robotic surgical tools to estimate the force exerted by the tools, thus solving the first and more critical part of the problem. The working principle opted for this sensor design is a change in the inductance values of the planar coils printed on a printed circuit board (PCB) when a magnetorheological elastomer (MRE) approaches it. The proposed sensor has a simple design, a soft contact surface, low hysteresis and minimum error, making it suitable for tactile force sensing. The proposed sensor is fabricated and tested with two different materials; silicon Ecoflex-30 and silicone RTV-528. Both variants provide different resolution, sensitivity, and force measurement ranges due to the different mechanical properties of the fabrication material. Finite element method (FEM) based analyses are carried out to design and optimize the sensor. A complete experimental characterization is performed to test the sensor's capabilities. The proposed tactile force sensor can measure forces applied in normal, shear, and planar angular directions. The sensor with Ecoflex-30 can measure forces up to 25 N and 2.5 N in normal and shear directions, whereas the sensor built with RTV-528 can measure forces up to 30 N and 6 N in similar directions. The proposed sensor can be employed in surgical tools as it has a small footprint and can measure higher forces, making it suitable for various surgical procedures.

Key Words: *Tactile sensor, tri-axis force sensor, magnetorheological elastomer, finite element method (FEM), inductance measurement*

Table of Contents

List of Figures

List of Tables

List of Journals/Conference Papers

Khalid, Muhammad A., Muhammad M. Saleem, Mohsin I. Tiwana, Rana I. Shakoor, and Rebecca Cheung. 2022. "Design and Characterization of Three-Axis High Range Inductive Tactile Force Sensor Utilizing Magnetorheological Elastomer for Robotic Surgical Applications"

(Submitted in IEEE Sensors Journal)

List of Abbreviations

PCB	Printed Circuit Board
MRE	Magnetorheological Elastomer
FEM	Finite Element Method
MIS	Minimally Invasive Surgery
RMIS	Robot-Assisted Minimally Invasive Surgery
PDMS	Polydimethylsiloxane
PVDF	Polyvinylidene Fluoride or Polyvinylidene Difluoride
MEMS	Microelectromechanical Systems
SOI	Silicon-On-Insulator
2D	Two Dimensional
3D	Three Dimensional
CAD	Computer Aided Design
PLA	Polylactic Acid or polylactide
PC	Personal Computer
GUI	Graphical User Interface
EMI	Electromagnetic Interference

Chapter 1: Introduction

Haptic feedback provides surgeons with necessary information during surgical procedures. It includes properties like stiffness and structural investigation of the patient's body tissues and internal organs with which surgeons interact through the surgical tools. This information is vital in performing a successful surgery as it guides the surgeon to manipulate the tools more safely and avoid excessive force application on any sensitive areas. With advancements in the medical field, robot-assisted surgeries are making their way by bringing advantages over conventional procedures. The lack of haptic feedback in robot-assisted practices is the area of current research. This chapter discusses the benefits of robot-assisted surgeries, the importance of haptic feedback, attempts to regain force and tactile sensing, and difficulties in achieving the objectives.

1.1 Minimally Invasive Surgery (MIS)

Minimally invasive surgery (MIS) is a type of surgical procedure which requires small incisions in a human body through which specially designed surgical tools are passed along with an endoscopic camera for visual presentation. A thin tube called a trocar that may or may not be flexible is inserted into the incision hole. The trocar houses a surgical instrument with a tool at one end and a surgeon's grip at the other end to perform surgical tasks. MIS offers many benefits over open surgeries, such as minimized invasiveness, less blood loss, reduced chances of infection, less after-surgery pain and short recovery time. Laparoscopic surgery is also a type of MIS. The main disadvantage of this surgical procedure is the long training times before surgeons get used to it. As the insertion points are fixed, the tools have limited access in adapting to different orientations and positions. A restricted movement puts stress on the surgeon's hand and builds fatigue and mental pressure, which can cause wrong moves and mistakes [1]. Also, it is complicated for a surgeon to estimate the force required to manipulate tissues as the tool tissue interaction feedback is compromised due to the friction of the tool shaft with the incision hole.

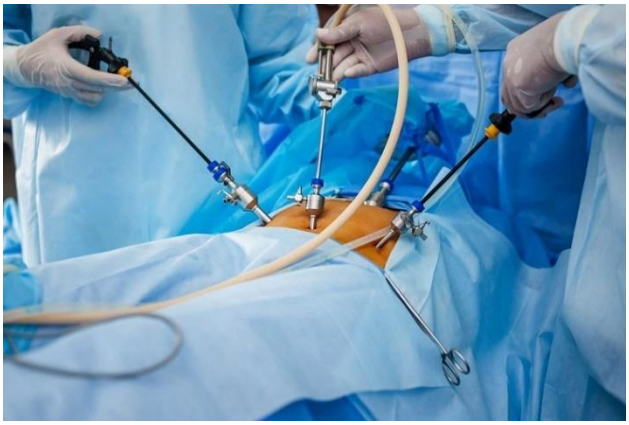

Figure 1. 1 Minimally invasive surgery (MIS) [2]

1.2 Robot-Assisted Minimally Invasive Surgery (RMIS)

MIS had space and manoeuvrability constraints which a robot assistance method has covered. The improved motion, accessibility, and elimination of surgeon's fatigue are major advantages offered by a robot-assisted minimally invasive surgery (RMIS). Researchers and surgeons are interested in this new field of research. The teleoperated RMIS systems include the ZEUST^{M} and the da Vinci^{TM} robotic surgical systems [3, 4], to name a few. These robotic systems have a configuration of master-slave where a surgeon sits in front of a computer console with in-hand controls for manipulating tools inserted in a patient's body at a distance. With RMIS, the performance of surgeries has improved and the field of work has also increased due to the additional degree of freedoms that newer tool shafts and robotic arms offer. These systems have increased the number and complexity of surgical procedures surgeons can perform. The surgeons do not have to hold heavy surgical instruments as robotic arms are powered devices and offer additional features like hardware damping and enhanced software signal filtration. With RMIS, surgeons are free from physiologic tremors and can have improved hand and eye coordination. While RMIS brings many benefits over the predecessor techniques, the high cost of surgical systems and the lack of force and tactile feedback from tool and tissue interaction remains a challenge [5].

Figure 1. 2 Robot-assisted minimally invasive surgery (RMIS) [6]

1.3 Feedback in Robotic Surgery

Feedback in robot-assisted surgical systems can be divided into force feedback and tactile feedback. Force sensing represents the amount of force applied by the surgeon through the surgical tool on the patient's tissue while performing a task. In contrast, tactile sensing provides information about different parameters and characteristics of the tissue and organs the tool interacts with physically.

1.3.1 Force Sensing

Force sensing is associated with measuring a force at a single point of interest or observing the resistance offered against a surface. In surgical systems, it is defined as the force experienced by the sensitive structures inside the patient's body when a surgical tool is inserted inside the body through tiny holes. The force must not exceed a safe amount; otherwise, tools cause damage to the healthy tissues and arteries in the body, which is not desired. A feedback system is required to transmit the sensed force to surgeons. Many highly accurate and robust commercial force sensors are available, but these cannot be used inside surgical tools due to the limitation of size. And commercial surgical systems do not offer a force feedback system which is essential. There are two ways to incorporate force feedback into the surgical systems; one is to make sensors that can be integrated into the existing tools, and the other is to redesign the tools for the surgical systems.

1.3.2 Tactile Sensing

Tactile sensing is related to the features of the skin. A tactile sensor may measure one or more properties from temperature, stiffness, vibration, shape, texture, vibration and normal and shear forces [7]. Sometimes, an array of sensing elements is used to estimate characteristics over an area of contact to achieve one of the properties. Tactile sensing has a wide range of applications. Haptic displays are a new and emerging field of research where a touch screen gives the user the feel of the actual object being displayed on the screen. A robotic hand and fingers integrated with sensors to estimate slippage and gripping force according to object stiffness. Surgical instruments in robotic surgery where integrated sensors are the only means to estimate the forces required for tissue manipulation [8]. One example in the medical examination is a palpation probe, where an array of sensing elements can discover any stiffness under the skin, hidden from the naked eye by creating a pressure profile at multiple points when touched to the skin area.

1.4 Challenges for Integrating Sensors in Surgical Tools

Technology always contributes to easing humans' lives, but there is a phase where it is in the process of research and development until it reaches a point of stability and comfort. The task of embedding force and tactile feedback in surgical tools is a bigger challenge and offers different limitations in different application areas [7]. In the biomedical field, any surgical procedure requires multiple tools insertion inside the human body to perform the procedure. The feedback sensor integrated surgical tool must possess the following features [9].

- Small size
- Aesthetic geometry shape
- Biocompatible
- Sterilizable
- Minimal cost of manufacturing
- Disposable or reusable

1.5 Transduction Principles of Tactile Sensors

There are many principles on which researchers have based their tactile sensors, including capacitive, piezoelectric, piezoresistive, inductive and optoelectric. A short discussion of how each of these principles works is mentioned in this section. Sensors based on these working principles, their advantages and limitations are discussed in chapter 2.

Capacitive sensors work on the principle of change in capacitance. There are two electrodes or conductive plates with a dielectric medium between them. A dielectric medium is an elastomer. Change in capacitance depends upon the area between the two plates, the distance between them and the properties of the dielectric medium. When a force is applied on the top plate, the distance between the two plates decreases due to elastomer deformation. The change in capacitance is mapped to the amount of applied force. Multiple pairs of capacitive plates can be used to make an array and different configurations can be adopted to differentiate between single or multi-axis input forces.

Piezoelectric sensors are based on the piezoelectric material. There are many piezoelectric materials available in the category of crystals and ceramics. The material is sandwiched between two metal plates, mechanical stress applied to the plates causes compression of the piezoelectric material, and in turn, electrons shift their position and start moving towards the plates, which is detected as the electric potential on the two plates. Piezoelectric materials have many applications in sensors and transducers. There is also an inverse piezoelectric phenomenon where an electric protentional is applied to the metal plates and pressure or stress is experienced by the piezoelectric material. This phenomenon has applications in acoustics.

Piezoresistive sensors work on the principle that the electrical resistance of the piezoresistive materials varies when a force or mechanical strain is applied to the material. Piezoresistive materials are metal or semiconductors like silicon. They are also available in flexible forms like foam and rubber sheets. They have applications in pressure, force and acceleration sensors. These are also being used in wearable sensors and tactile sensing.

Optoelectric sensors are composed of a light source, a modulator (transduction element) and a light detector. Light from a light source is transmitted by means of optical fibers to the medium where it passes through and is detected by the photodetector or camera at the other end. When a force is applied on the contact side of the sensor, light shift and refracts because of the deformation in the elastic medium, the shift in the intensity or spectrum is detected at the other end.

Inductive sensors are composed of a primary coil, an elastomer and a secondary coil. A secondary coil can additionally either be a copper plate or a magnetorheological elastomer. The primary coil is excited by an alternating current which generates a magnetic field around it, reaching the secondary coil. A magnetic coupling exists between the two coils, which is affected when a force is applied on the sensor. This in turn, changes the primary coil's inductance value, and a corresponding input force can be mapped accordingly.

Magnetic sensors work by detecting a change in the magnetic field intensity. Its structure consists of a small size permanent magnet and a Hall sensor underneath with an elastomer in between them. A force applied on the elastomer deforms it and three-dimensional displacement of the magnet is recorded by the Hall sensor as the change in magnetic field flux. Multiple pairs of permanent magnets and Hall sensors are used in a particular configuration to estimate contact forces.

There are other force-sensing mechanisms, strain gauges, current-based and displacement transducers. Strain gauges are small beams embedded in an elastomer that measure mechanical strain, and these are commonly used in a configuration of a Wheatstone bridge. The current-based sensing technique utilizes the motors in the robotic grippers and medical instruments and monitors their current values to detect forces and torques. Displacement transducers are used for displacement measurement where an elastic medium is a linear spring; by knowing the spring stiffness, a force can be estimated.

1.6 Examples of Use of Force and Tactile Sensors in the Medical Field

1.6.1 Palpation Probe

Palpation is a method of inspecting using fingers in a physical examination to investigate the possible presence of a tumor under the skin. A palpation probe is built and attached to a master-slave system with a tactile sensor on the tip of the probe and a force sensor at the back end. The study investigates the force applied for the localization of artificial tumors by a human and a tactile probe. The data analysis shows that the force applied by the probe is 55 percent lesser on average than the force applied by a human and an improvement in the tumor localization accuracy by 50 percent is also observed [10]. Such a compact tactile probing system can also be used in MIS to recognize uneven tissue stiffness.

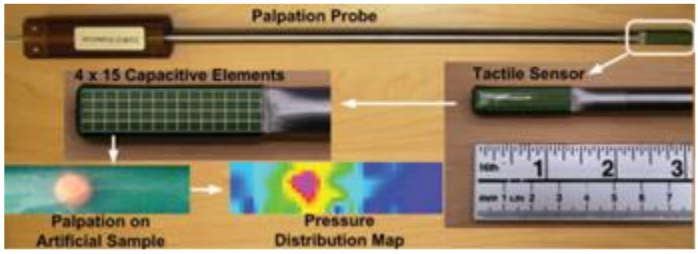

Figure 1. 3 Palpation probe [10]

1.6.2 Laryngeal Force Sensor

Laryngoscopy is used in the examination of the larynx and pharynx. It is a usual surgical procedure to remove any vocal cord lesions (tumor and ulcers). There is no means of estimating the safe limits of force that the internal organs can bear by the movement of the surgical tools in a limited and critical environment. There have been reports and research in which several types of complications have been documented. The after-surgery complications include tongue pain, inflammation, dysphagia, numbness, taste modifications and nerve damage. Research is conducted where an externally mounted force sensor is used to estimate the forces applied on a wide variety of patients during the surgery and the after-effects on each of them. An EAT-10 score (Eating Assessment Tool) was noted for each patient after the surgery. It was found that excessive force is a major contributor to the complications in patients with abnormal EAT scores [11].

Figure 1. 4 Laryngeal force sensor [11]

1.6.3 Surgical Forceps

A surgical forceps integrated with a force sensor and capable of measuring grasping and pulling forces during surgical procedures is an important example. The sensor has capacitive tactile sensors embedded in the jaws of forceps. The forceps are attached to a surgical system and relevant force measurements are carried out to show the usefulness of these modified forceps for minimally invasive robotic surgeries [12].

Figure 1. 5 Force sensor integrated surgical forceps [12]

1.6.4 Sensorized Endoscope

An endoscope is used in many medical examinations and surgical procedures. It usually provides only a camera feed. An effort is made to upgrade it to be used to diagnose a possible submucosal tumor. It is made with a hard tip of a copper ball encapsulated with a polydimethylsiloxane (PDMS) material and polyvinylidene fluoride or polyvinylidene

Figure 1. 6 Sensorized endoscope [13]

difluoride (PVDF) polymer as a sensing medium. This tactile endoscope can improve treatment time and quality [13].

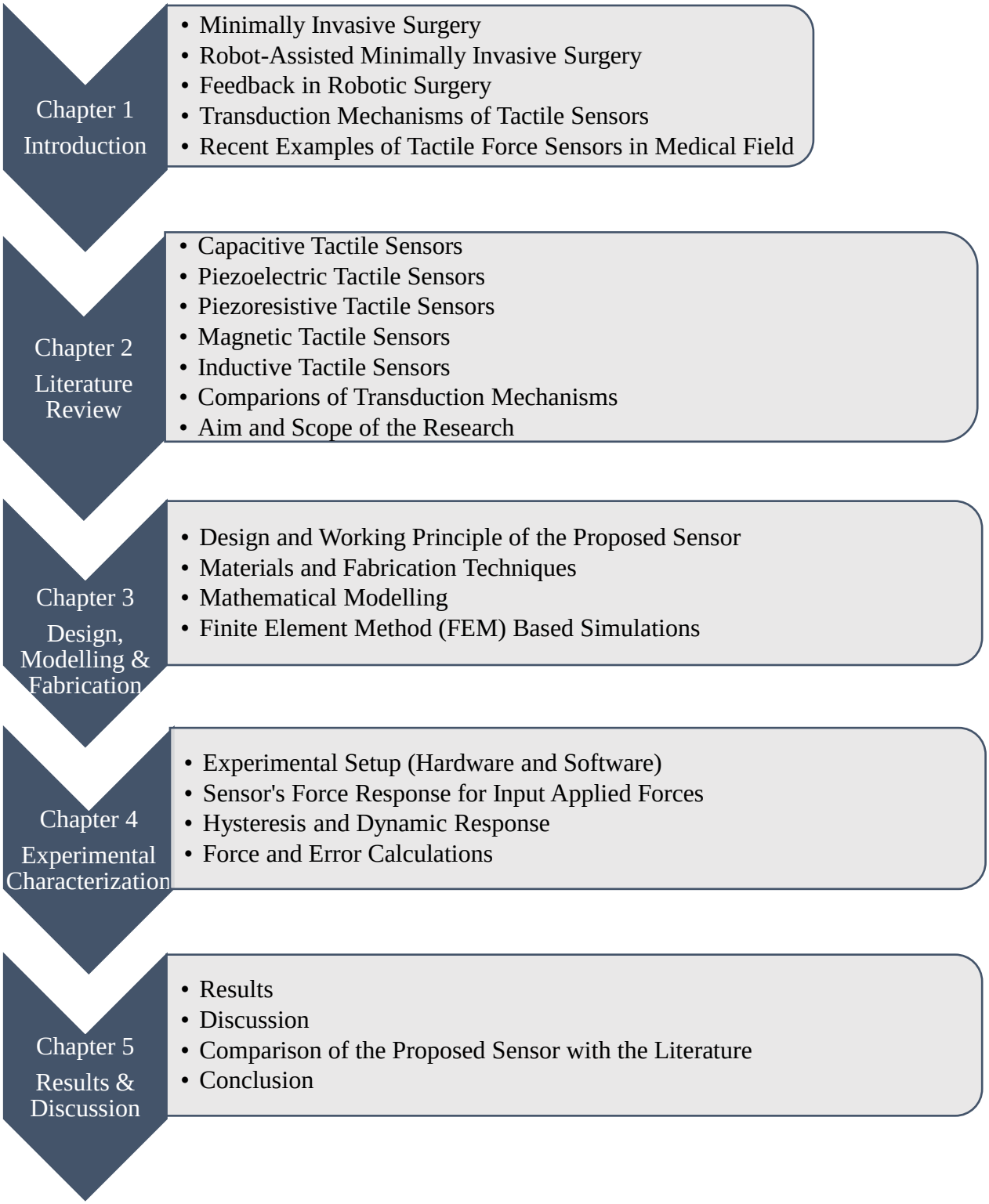

Figure 1. 7 Flowchart of the Research

Chapter 2: Literature Review

This chapter comprises a review of tactile sensors from the literature. The tactile sensors for force estimation are discussed only. A comparison is made between different working principles of tactile sensors to understand the advantages each of these principles offers and their limitations for the application of robotic surgery. Finally, a solution that solves the current limitations is proposed, which is the ground of this work.

2.1 Tactile Force Sensors from the Literature

In the literature, there are multiple transduction mechanisms used to estimate force. A short introduction to the construction and working principles of various mechanisms is already covered in the previous chapter. A general structural composition always has an elastic medium (elastomer) inside a sensor which deforms when a force is applied. There is also a sensing mechanism that transfers a mechanical force into another physical quantity which is measured, filtered and recorded by means of a data acquisition system. Tactile force sensors can either be single-axis or three-axis, depending on their design and application requirements.

2.1.1 Capacitive Tactile Sensors

A tri-axial capacitive sensor is made in an array configuration. It consists of overlapping electrode pairs of copper-clad Kapton lamination with a patterned elastomer made of silicone. The unit cell in the array is capable of measuring normal and shear forces and two-dimensional (2D) and three-dimensional (3D) shear force angles. When a force is applied on the contact surface of the sensor, the top plate deforms and hence the overlapping area of the electrode pair shifts. The sensor can measure force both in normal and shear directions with a range of up to 20 N with a linear response region of 10 N [14].

Another capacitance-based tactile sensor is built with a 2 × 2 electrode pair configuration, comprising of 4 planar capacitors for measuring normal and shear forces. It also has a partially filled elastomer layer that displaces downwards or sideways depending on the

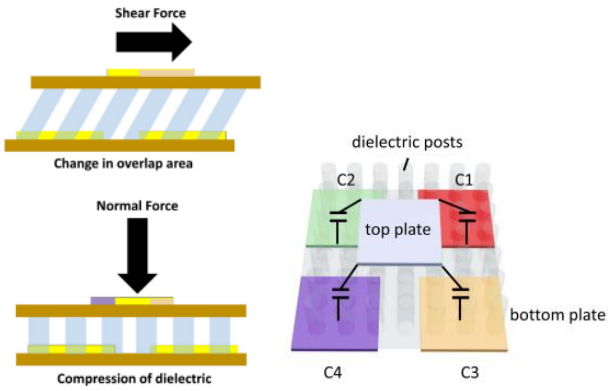

Figure 2. 1 Three-axis capacitive sensor for shear force detection [14]

type of force applied to it. It also has short height posts between electrode plates which are engaged when the force exceeds a certain threshold. This approach makes this sensor highly sensitive to small forces and also makes it a high dynamic range force sensor. This sensor can measure forces up to 2.1 N [15].

A recent development in capacitance-based tactile force sensors proposes a flexible array-less design for applications in electronic skins. Instead of an electrode pair array, the design utilizes layers of electrode pair with a dielectric layer between them. The dielectric is made of a mixture of PDMS and carbon nano tubes in a particular ratio. The electrodes are made of conductive silver glue. The electrodes are further encapsulated in PDMS layers on top and bottom. The contact force causes a deformation in the structure and disturbance in the electric potential of the electrode plate. The redistribution of electric charges in the dielectric medium is observed to estimate the position and magnitude of the applied force [16].

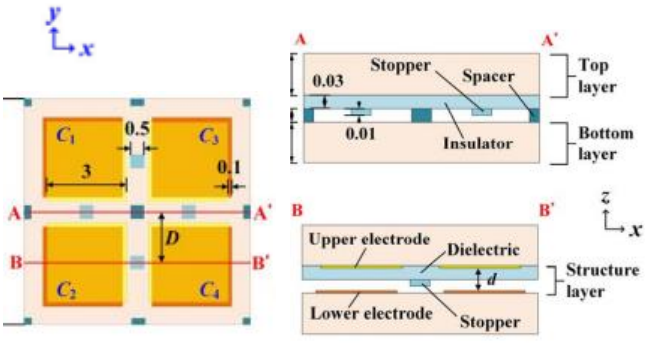

Figure 2. 2 Multistage capacitive tactile sensor [15]

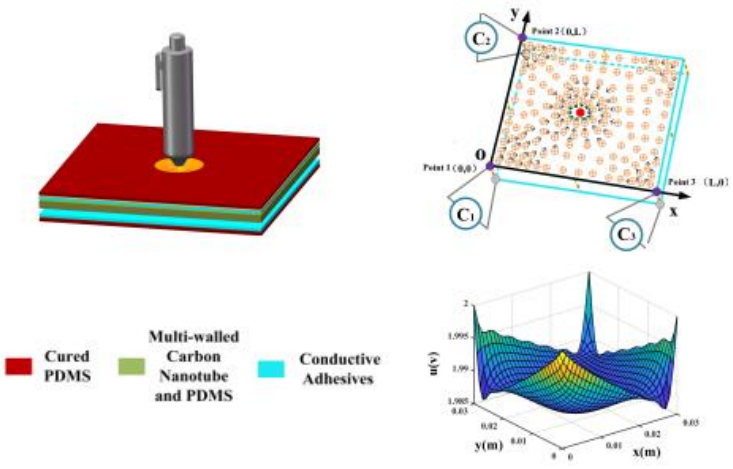

Figure 2. 3 Array-less capacitive tactile sensor [16]

2.1.2 Piezoelectric Tactile Sensors

A tactile sensor for hard tissue detection is built using a catheter robot in MIS. This sensor has a diameter of 8 mm. Catheter-based palpation must meet a size constraint, so the fabricated sensor has an overall diameter of 8 mm. sensor has a spiral shape and a piezo transducer in a vertical configuration. This design helps in low-frequency operation, which is a requirement in testing biological tissues. The sensor can sense hardness in the range of 0–1.7 MPa while operating at a low-frequency range. An ex vivo experiment is run for the comparison and it affirms that the sensor is capable of detecting the presence and shape of an embedded lump. Major achievements are a small sensor size, low-frequency operation, simplified proposed data acquisition and measurement technique, and easy integration into MIS tools [17].

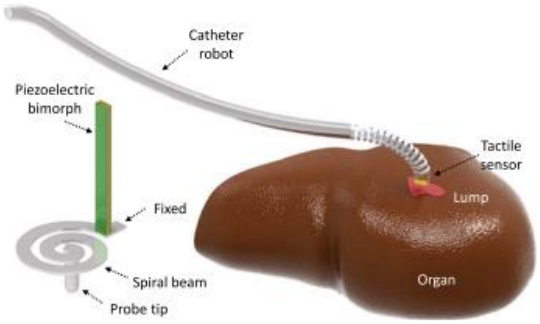

Figure 2. 4 Spiral piezoelectric tactile sensor for tissue hardness palpation in MIS [17]

Another piezoelectric tactile sensor for measuring tissue stiffness in RMIS is presented. It can measure the stiffness when the probe is pressed vertically against the tissue and also when the probe is approaching the examination area at an angle. It solved the limitation of previously existing sensors' which only supported vertical contact sensing. This sensor can detect stiffness at an angle ranging from 0° to 45°. Simulation and experimental results are in close range. This improved palpation probe works better and is close to the natural behavior of humans. The recognition rate for angles under 30◦ is 100% and is 94.1% for angles within 45◦ [18].

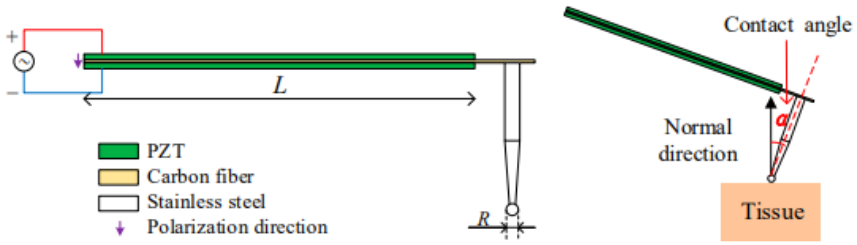

Figure 2. 5 Piezoelectric tactile sensor for stiffness detection at arbitrary angle [18]

A piezoelectric-based tactile sensor in array configuration is made in five layers inspired by the multilayer structure of human skin. It has three layers of PDMS and two layers of PVDF. The middle layer of PDMS separates two PVDF layers and helps distinguish the type of input disturbance. There are electrode pairs for the detection of electric potential due to deformation in the structure. Each PVDF layer either undergoes tension or compression. The sensor can sense pressure and bend based on the fact that during

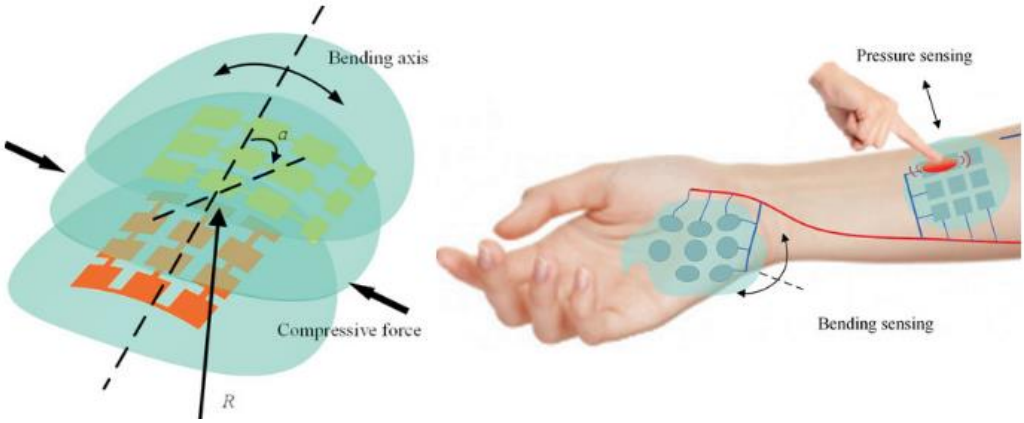

Figure 2. 6 Multilayer piezoelectric based tactile sensor [19]

pressure application, a major potential change occurs in the top PVDF layer whereas, during bending application, a more visible change is detected in the bottom layer of the PVDF. This sensor can be used for health monitoring [19].

2.1.3 Piezoresistive Tactile Sensors

A tri-axial tactile sensor capable of measuring normal and shear stress is presented. This is a Microelectromechanical system (MEMS) and the sensor is made on a silicon-on-insulator (SOI) wafer. The sensor is made of a metal structure with three piezoresistive beams. These beams are doped with silicon on top for one beam and on the side for two beams; one beam functions for normal sensing and the other two for shear sensing. The sizes of the beams are in µm. The sensor chip is enclosed in a PDMS sheet and the overall size of the sensor is 2 mm × 2mm × 0.3 mm. The sensor can measure normal and shear stress up to 400 kPa and 100 kPa, respectively. The sensor's response is found to be linear with little to no cross-axes interference due to a decoupled sensing scheme. This type of tactile sensor has applications in robotic tactile sensing [20].

A new design of piezoresistive tactile sensor based on cantilever beams is presented where beams have a free field of motion underneath them against the applied forces, unlike conventional sensors where the surrounding elastomer restricts the movement of beams. This is a MEMS sensor with a small footprint and simpler instrumentation. When pressure is applied, a microstructure made of PDMS moves the cantilever beams in a normal or lateral direction based on the direction of the applied force. The extent of bending of the beams differentiates the direction of applied pressure. The results display an increased sensitivity of 150 times for normal forces and 100 times for lateral forces [21].

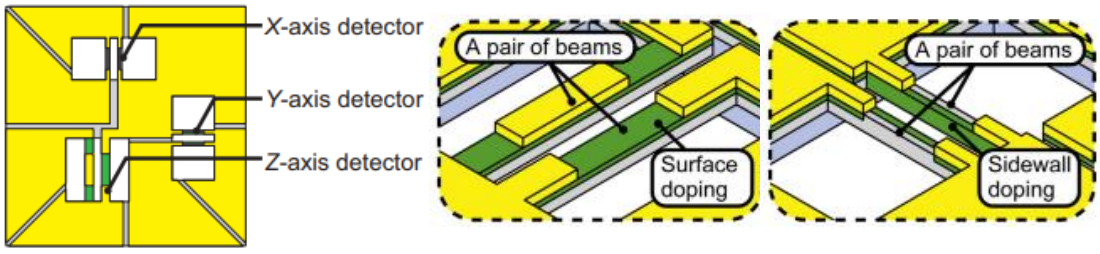

Figure 2. 7 Piezoresistive tactile sensor without crosstalk [20]

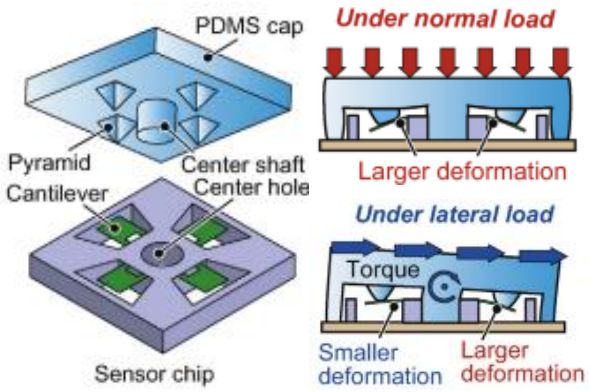

Figure 2. 8 Highly sensitive three-axis tactile sensor using piezoresistive cantilevers [21]

A piezoresistive tactile sensor with multi-walled carbon nanotubes is also reported in the literature. It utilizes a grid-type structural layer made of PDMS and carbon nano tubes. An electrode made of silver functions as a sensing layer and a protection layer made of PDMS is used for physical interaction. Carbon nano tubes make this sensor an active piezoresistive sensor that operates in the presence of external electric voltage. The resistance of the sensing medium corresponds to a current path through connected tubes which changes on pressure variation. The concentration or the doping amount of carbon nano tubes affects the performance and different parameters of the sensor [22].

2.1.4 Magnetic Tactile Sensors

A tri-axis magnetic tactile sensor is presented which is used as a skin sensor for robots. It mainly comprises permanent magnets and magnetic field sensors. A 3-axis magnetic field sensing IC MLX90393 is used for estimating the 3D displacement of the permanent

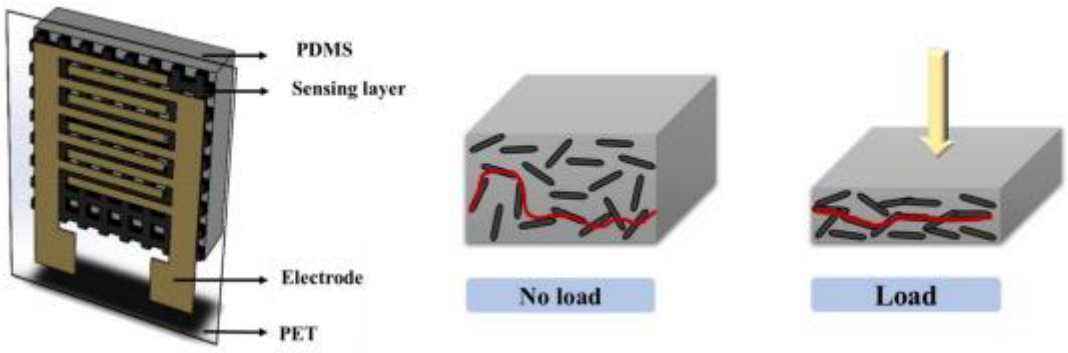

Figure 2. 9 Piezoresistive tactile sensor based on carbon nano tubes [22]

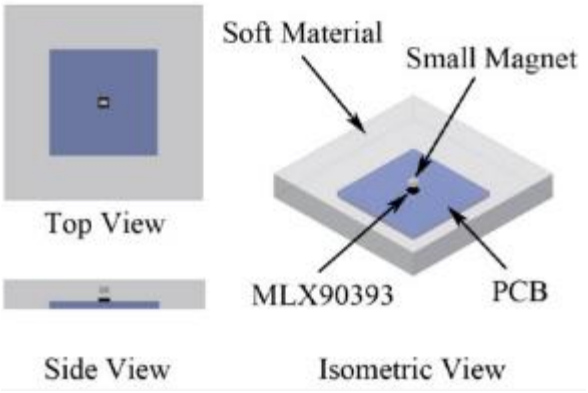

Figure 2. 10 Hall effect-based soft skin sensor [23]

magnet. Magnet and IC are vertically aligned and silicone rubber as the elastomer resides between them to support the magnets. Magnetic field lines originate from the magnet and end in the hall sensor and their intensity varies by the disturbance in the magnet's position. The experiment conducted showed that the sensor could differentiate force components. Also, change in the magnetic field due to temperature is studied and the drift is compensated using a temperature sensor. The sensor's resolution is 9.8 mN and a maximum force of 14.22 N is measured [23].

The application of tactile sensors as electronic skin is of high importance. Another tri-axis force sensor for robot skin is presented. This sensor is simple in construction with low-cost components and is capable of both normal and shear force measurement. The author made an array using a flexible PCB and fabricated it in a shape of a fingertip for a robot. The sensor is tested for normal and shear forces up to 6 N and 1 N, respectively. The sensor promises acceptable hysteresis with a low signal-to-noise ratio. The sensor is

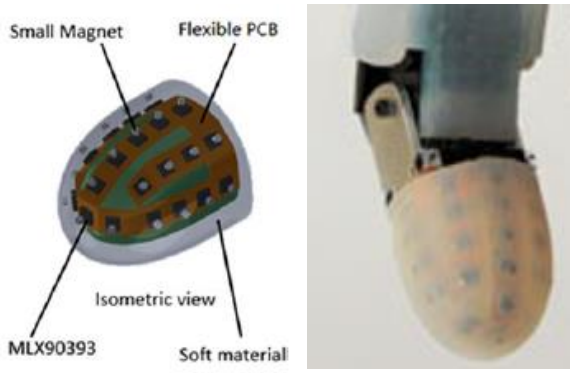

Figure 2. 11 Soft electronic skin for robotic hands [24]

mounted on a commercial robot system and experiments showed promising possible use in the gripping and shape estimation of objects. This tactile force sensor is an important feature for robots with gripping applications to avoid excessive force and eliminate slippage by providing force feedback [24].

A magnetic tactile sensor with simple components like soft magnetic film, elastomer layer and a hall sensor underneath is fabricated. The working principle says that the deformation in the magnetic film causes a change in the magnetic flux density monitored by the hall sensor. The array-like configuration of the closely placed unit cells helps distinguish the normal and shear forces. The author has tested the sensor prototype for robotic grasping and needle threading application in teleoperation. The sensor's response depicts a decoupled force relation and high-resolution force sensing [25].

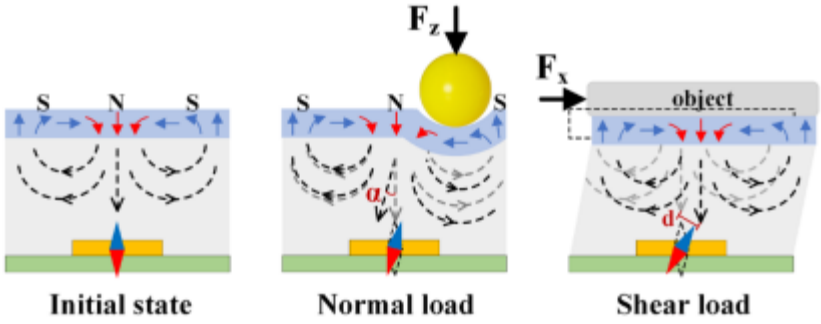

Figure 2. 12 soft magnetic tactile force sensor [25]

2.1.5 Inductive Tactile Sensors (Rigid Contact Surface)

Recently, there has been an increased interest in inductance-based force and tactile sensors. The idea fundamentally originated from Eddy-current sensors [26], [27], which are widely used for non-contact detection of metal objects in proximity and displacement measurement [28], [29]. Inductive sensors are based on an LC circuit and when a metal is sensed in its proximity, the resonance frequency of an LC circuit changes. A detailed working mechanism is that a circuit has coils that are energized with an alternating current which creates magnetic field lines around the coil. The magnetic field lines reach the Aluminum disc right above the coil and eddy currents are induced in the disc. These eddy currents will form their own magnetic field, which will interfere with the original magnetic

field of the coils. The change is detected in the inductance value of the coils through relevant electronic boards. This phenomenon is supported by Faraday's and Lenz's law of electromagnetic induction. Examples of inductance-based tactile sensors from the literature are stated below.

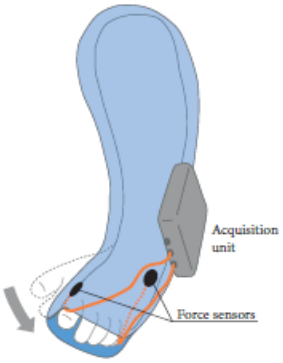

Figure 2. 13 Single axis inductive force sensor [30]

A single-axis inductive force sensor for force measurements in Dupuytren fingers and clubfeet treatment was communicated in 2018. In a newly born with a curved foot, a cast is applied on it along with the sensor which is required to change frequently as the bones are soft and adaptable. A force sensor senses the change in pressure applied by the bone on the sensor. This efficient monitoring defines the cast change intervals. The sensor can measure forces in the range of 0-10 N with a resolution of tens of mN. It showed good functioning for long-term force measurements [30]. In 2018, Wang, et al. [31] presented a single axis inductive tactile sensor that is based on the eddy-current effect. The sensor has a simple construction with three main components. A planar dual-layer spiral coil printed on a flexible PCB, an elastomer above it and an Aluminum film on top as the sensing target. Coils are arranged in 4 × 4 format with a single coil of Ø8 mm. The sensor works in a way that when force is applied on the Aluminum disc, it displaces downwards,

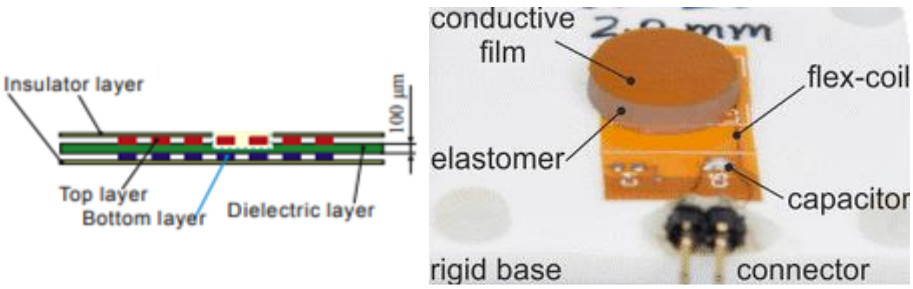

Figure 2. 14 Inductive tactile sensor based on eddy-current effect [31]

causing an inductance change of the coils which is then mapped with the input applied force. The unit cell demonstrated 0.82 mN resolution with a force range over 15N.

In 2018, Wang, et al. [32] also stated an upgraded version in the form of a tri-axis inductive tactile sensor using the same eddy-current effect. The sensor consists of four copper coils printed on a flexible PCB and arranged in a 2 × 2 matrix form. The elastomer is made with Ecoflex and covers the four coils. An aluminum film is glued on top of the sensor that acts as the sensing target. The circuit consists of an inductor (coil) and a capacitor, thus forming an LC circuit. The circuit's resonance frequency is continuously monitored and each coil's inductance is calculated. The gap closing and an overlap increase between the film and coils decrease the inductance of the coils. The force in normal or shear direction is estimated through different combinations of inductance variations in the four coils. This sensor has a size of Ø14 × 2 mm and can measure applied normal forces up to 13 N and shear forces up to ±0.7 N with a resolution of 0.3 mN. This sensor can be used in grippers for grasping, slippage detection and force sensing in robotic instruments.

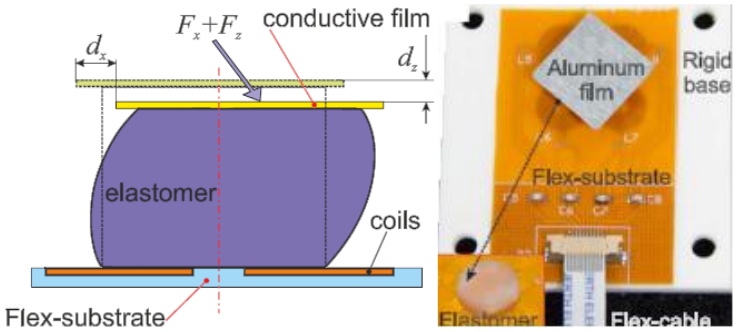

Figure 2. 15 Tri-axis soft inductive tactile force sensor [32]

In 2020, another researcher reported a three-axis inductive force sensor for measuring plantar normal and shear load to monitor the development of diabetic foot ulcers (DFUs), an important application in the medical field. The construction of this sensor is similar to the previously reported inductive tactile sensor. It mainly consists of four dual-layer square-shaped spiral coils with a cylindrical elastomer made of Ecoflex on top of the coils and a disc-shaped circular aluminum sensing target. The target is placed in the center of a 2 × 2 matrix array of coils at a vertical height of 2 mm and overlaps all coils partially. The

sensor also works on the previously reported mechanism by detecting changes in the inductance values of the coils. A normal force applied to the sensor compresses the elastomer and moves down the target and a shear force causes a change in the overlap area between the target and coils. The target displacement changes the resonance frequency of each coil in the circuit which is used to calculate the inductance of the coils. The author also studied the effect of different shapes of inductors (elliptical, circular and square), the number of inductors and the coil loop density. This sensor works on the eddy-current principle and can measure normal and shear contact forces. A complete prototype of an in-shoe sole is made and characterized. The sensors array showed a promising force measurement range of 0-106 N and ±16 N for normal and shear directions, respectively, satisfying the particular medical application's requirement [33].

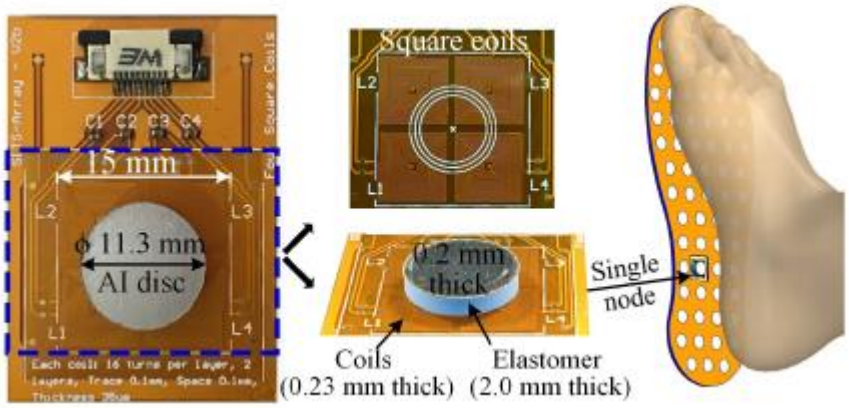

Figure 2. 16 Inductive force sensor for in-shoe plantar pressure measurement [33]

2.1.6 Limitations in Present Inductive Tactile Force Sensors

Eddy-current-based flexible tactile sensors presented earlier though provide good resolution and decent force ranges but a major constraint they offer is the non-flexible contact surface which limits their use in applications where a soft and elastic contact surface might assist the application, especially in medical diagnostics and robotic surgery where a force sensor integrated instrument may get in contact with human skin or internal organs.

2.2 Comparison of Transduction Mechanisms

Table 2.1 Comparison of different transduction mechanisms [7, 34]

Mechanism	Advantages	Limitations
Capacitive	High-frequency response Good special resolution Large dynamic range High sensitivity	Noise suspectable Stray capacitance Complex measurement circuit Crosstalk
Piezoresistive	High spatial resolution Fewer electronics Low cost Less susceptible to noise	Suffer from hysteresis Lower repeatability High power consumption
Piezoelectric	High-frequency response High sensitivity High accuracy High dynamic range	Measure dynamic forces only Poor spatial resolution Charge leakages
Optoelectric/ Optical	High repeatability High spatial resolution Good reliability Good sensing range Immunity from EMI	Bulky in size Non-conformable Susceptible to misalignment
Magnetic	Linear output High dynamic range Highly Reliable	Magnetic interference Temperature drift
Inductive	High power output High sensitivity High dynamic range Linear output	Low-frequency response More power consumption

2.3 A solution from the Literature (Soft Contact Surface)

A researcher presented a solution to deal with the limitation experienced in the inductive tactile sensors. The researcher has addressed the above issue by replacing the hard conductive film in eddy-current-based sensors with a Magnetorheological material. The rheological properties of this material vary when it experiences a magnetic field. Magnetorheological materials (MRE) are ferromagnetic and have high relative permeability. This changes the working mechanism of the inductive sensors with a huge shift. Conventionally, when a metal target approaches the coil, the resonance frequency of an LC circuit increases and the inductance of the coil decreases due to the eddy-current phenomenon, whereas, now, with the MRE block (sensing target) approaching the coil, it acts as the magnetic core for the coil which decreases the resonance frequency of the circuit and in turn increases the inductance value of the coil. This magnetic coupling is different from the previous bonding between the metal target (copper disc) and the coil. The author has made a three-axis tactile force sensor with a cylindrical shape. At the base of the sensor, there are four dual-layer planner spiral coils printed on flexible PCB. Above the PCB is an elastomer with a size of Ø30 x 10 mm. The elastomer holds the MRE block of size Ø15 x 3 mm in place. Elastomer is made up of silicone rubber and marker has a composition of silicone rubber and iron particles mixture. Silicon rubber and MRE block (also called ferromagnetic marker) possess flexible and soft contact surfaces. The author claimed that the sensor can measure normal forces (in Z-axis) up to 30 N and shear forces (in the X and Y-axis) up to ±8 N with sensitivities in a few hundred mN in each direction [35].

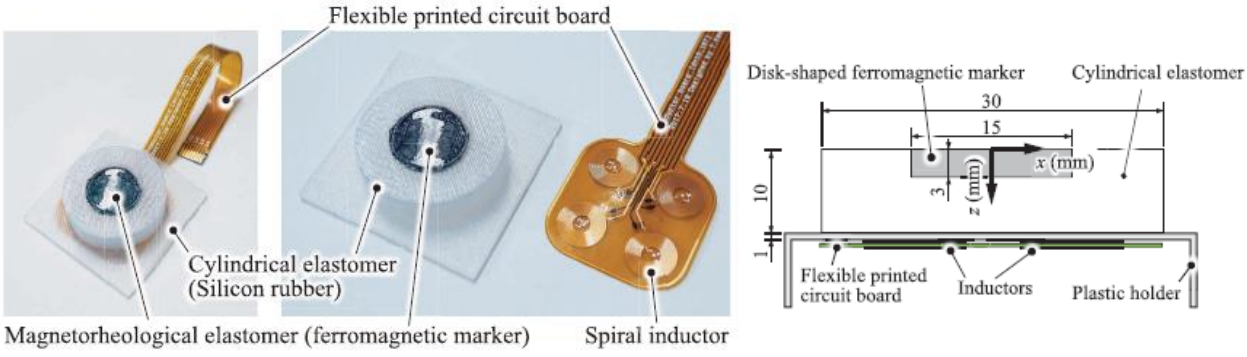

Figure 2. 17 Tactile sensor with a magnetorheological elastomer as the sensing material [35]

2.3.1 Redesigning the Solution for RMIS

This research work aims to design and develop a tactile sensor that can be used in RMIS. RMIS requires the sensor to be of small size, have good resolution and have a high enough force range for a wide range of surgical procedures. The closest approach which overcomes the limitations of different transduction mechanisms and holds the promise for further improvement is discussed in the previous section [35].

Although the given inductive sensor design sensor offers a soft contact surface, it has two major weaknesses: its large size and very low resolution [35]. A sensor with a size of 30 mm diameter and resolution of around 300-400 mN is not nearly appropriate for the RMIS application. A complete sensor redesign is required, which must address the above issues.

This work presents an MRE-based inductive tactile force sensor. All phases of the work like design, mathematical modeling, simulations, fabrication, experimentation and results analysis are dealt with in great detail. The design has many features not present in the literature, making it a unique high performing three-axis tactile sensor that can be used in RMIS application. The sensor is designed with an aim to be incorporated in surgical tools at a later stage or at least provides the basis for future work. The main features of the proposed sensor are mentioned below.

- Introduces a new configuration of the four sensing coils
- Uses optimized shape and size of the planar coils which enhances the sensitivity
- Introduces a patterned elastomer for better sensitivity
- Offers better resolution
- Has smaller size
- Decoupled contact force response
- Measures forces in normal (Z-axis) and shear (X and Y-axis) directions
- Introduces shear angles measurement from different directions
- Tested with two grades of liquid silicone rubber
- Low hysteresis
- Minimal error for larger forces

The next chapters cover complete details of the features mentioned above and different phases of the design and development of the proposed sensor.

Chapter 3: Design, Modelling and Fabrication

This chapter discusses the design and development of the proposed inductive tactile force sensor in detail. A design with a new configuration of sensing mechanism is presented in comparison to the literature. Then the materials used in the fabrication and fabrication process itself are explained. The mathematical model of the sensor and results from relevant Finite Element Method (FEM) based simulations are also discussed. Different aspects of optimization in various parameters are also expressed in each section.

3.1 Working Principle

The proposed sensor has four dual-layer copper coils printed on a PCB. An elastomer is placed and centered on top of the coils that hold the MRE block (ferromagnetic marker or marker). The marker is at a specific distance from the coils initially by the support of elastomer and it overlaps each coil equally. The elastomer and the marker behave as a single entity and are compressible soft materials. The marker is the sensing material and the elastomer just holds it and supports its movement in 3D. The graphic for the sensor design is shown in figure 3.1.

Each coil has a parallel capacitor in the circuit, making it an LC circuit (circuit with an inductor and capacitor with negligible resistance). The energy in the LC circuit is continuously shifting (resonating) between two types, potential energy stored across capacitor plates and current passing through the inductor. This circuit operates at a resonance frequency in megahertz. The sensor is powered with a low AC voltage which continuously generates changing magnetic field around the coils. The marker has the property that when it experiences a magnetic field, it's magnetized and its particles start aligning their magnetic field with the magnetic field of the source and it causes a change in the resonance frequency of the circuit. The inductance of the coils is calculated from the resonance frequency by knowing the value of the capacitor. The inductance value of all coils is monitored continuously. When a force in the normal direction (-Z-axis) is

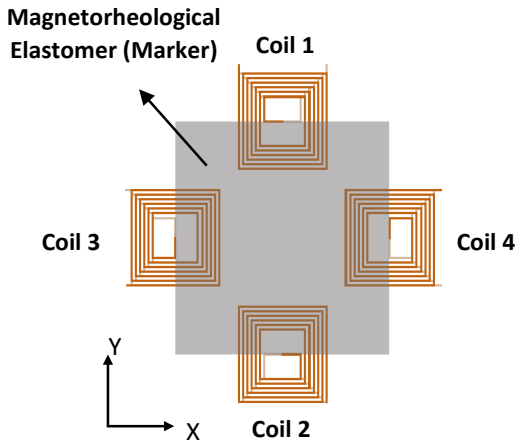

Figure 3. 1 Schematics of the proposed sensor (top view)

applied, the elastomer deforms uniformly; the compression also moves down the marker and closes some distance between the marker and the coils, causing a change in the inductance of all coils. In normal force, the change is an increase in the inductance value of all coils. When a shear force, for example, in the +X-axis is applied on the surface of the elastomer, the marker moves horizontally in the direction of the applied force. This movement causes an increase in the overlapping area of marker and coil 4 and a decrease in the overlapping area of marker and coil 3 and no change for coil 1 and coil 2. A similar trend is observed in the inductance values of the respective coils. Similarly, when an angular in-plane force is applied, for example, towards the first quadrant, the overlapping area and hence the inductance of coils 1 and coil 4 increases, whereas an opposite change in overlapping area and inductance of coils 2 and coil 3 is observed. The change in inductance values of four coils is formulated to easily differentiate the type of force (normal, shear, angular), amount of force, and the direction of a force. Table 3.1 shows the trend of change in inductance of all coils when normal, shear and angular forces are applied to the sensor from different directions. It covers all possible force application directions for which the sensor is designed. L_1, L_2, L_3 and L_4 represents inductance values of coil 1, coil 2, coil 3 and coil 4, respectively.

Table 3.1 Inductance change in coils against applied forces

Applied Force		Inductance Change			
		L_1	L_2	L_3	L_4
Normal	-Z	+	+	+	+
Shear	+X	♦	♦	-	+
	-X	♦	♦	+	-
	+Y	+	-	♦	♦
	-Y	-	+	♦	♦
Shear Angular	45°	+	-	-	+
	135°	+	-	+	-
	225°	-	+	+	-
	315°	-	+	-	+

3.2 Sensor Design and Fabrication

The proposed sensor has a simple construction and consists of three parts other than sensing electronics: the sensing coils, elastomer and the marker. The design and fabrication details of each part are mentioned in this section. A computer aided design (CAD) model depicting different components of the sensor is shown in figure 3.2.

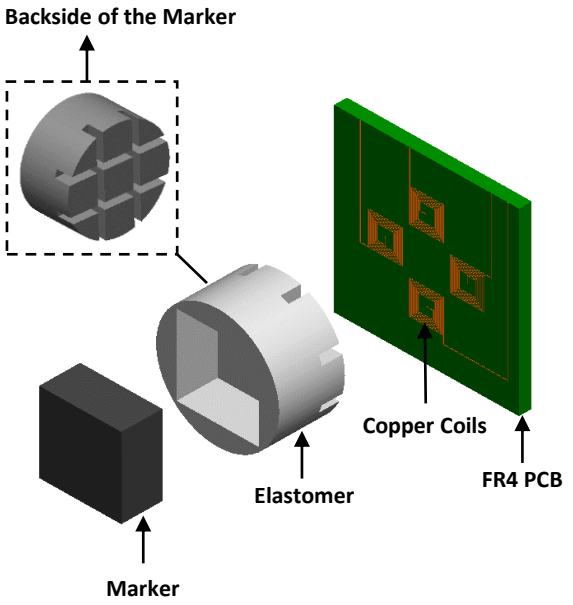

Figure 3. 2 Exploded CAD model of the proposed sensor

3.2.1 Sensing Coils

The base of the propose sensor is a layer made of 1.6 mm thick glass-reinforced epoxy laminate (FR4) which is a rigid type of PCB. FR4 has many benefits which makes it suitable for many electronic applications. FR4 is; low cost, lightweight, has high strength-to-weight ratio, has moisture and heat resistant properties and possesses low electric loss profile. The four dual-layer coils are printed in a plus configuration on the PCB. The shape and size of the coils are optimized through the literature study [33]. The study proves that the longer the length of the wire is, the higher its initial inductance value is. So, a square spiral shape coil design has a longer length of wire than the circular spiral shape in the same area. Also, considering a dual-layer coil design, the length and hence the initial inductance value of the coil increases by a decent amount. The coil is designed so that the coil from the top and bottom side of the PCB are connected in the center and make up a single wire with one terminal on top and the other on the bottom side of the PCB.

PCB of the proposed sensor is designed in Proteus PCB Design Software. It is manufactured by a commercial PCB prototyping service in China. The coil traces on the PCB are made of copper, vias of PCB have copper deposit in them, silkscreen is applied for marking and terminal tagging and both sides of PCB have a solder mask layer in green color which protects the PCB from short circuits. The trace width and gap of the coils are the most important design features in the whole work. The trace width is the width of printed copper wires in the coil and the trace gap is the distance between the consecutive wires, both of these are kept at 100 µm, which is the minimum achievable size for a rigid PCB by the manufacturer and it also matches with the literature. The thickness of the copper layer on PCB is kept at 35 µm. The area occupied by a single coil on PCB is 4.2 mm × 4.2 mm, with each coil having 6 full turns on each side of the PCB. The overall sensing area of the proposed sensor is 15 mm in diameter. The top view of the manufactured PCB and the schematic of a single coil is shown in Fig. 3.3.

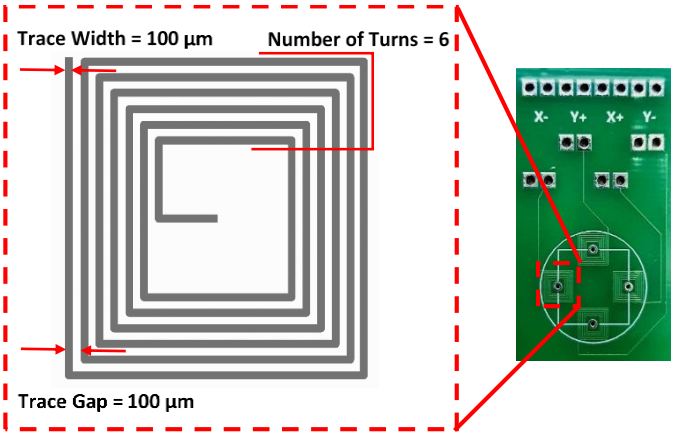

Figure 3. 3 Manufactured PCB (top side) and detailed schematics

3.2.2 Elastomer

Elastomer is a soft substance and it is a type of silicone-based polymer. In the sensor design it behaves as the separator between the marker and the coils. The design of the elastomer is improved as the solid cylindrical elastomer used by most researchers till now offers a disadvantage of undesired deflection. Previously, whenever a shear force is applied, the sensor detects some deflection in the normal direction, making it difficult to differentiate between different types of forces due to crosstalk among different axes and force measurement errors. Also, a solid elastomer offers low sensitivity for the applied force due to less elastomer deformation. The elastomer design is optimized and a patterned shape is introduced to solve it. A patterned elastomer has a posts-like shape at the bottom side, making its fill factor less than the solid elastomer and less contact area with the PCB, it is shown in figure 3.2. A patterned elastomer works in a way that it allows more deformation in the elastomer for the applied normal and shear force. The new design minimizes the undesired deflection and increases the sensor's sensitivity while sustaining a high enough force measurement range. Common knowledge and the literature both verify this approach [34].

The fabrication of the elastomer is done in the department's lab by following proper safety aspects and product guidelines. As mentioned earlier, two different types of sensor prototypes with two different elastomers are made. One elastomer is made with a famous silicone liquid rubber, Silicone Ecoflex-30, a product of Smooth-On, a USA-based

company and 30 in the name represents its shore hardness. Exoflex-30 is available in two parts (A and B) with a frosted transparent color. The two parts are measured by volume in equal proportion and mixed at a room temperature for 3 minutes. After that, degassing is performed and then the mixture is poured into the mold to cure. Cure time for Ecoflex-30 is about 4 hours which can be reduced by exposing it to higher temperatures. The second elastomer is made with a silicone liquid rubber, RTV-528. RTV-528 has white color and comes with a curing agent which can be added to the liquid silicone at 1 – 3%. The curing agent is added dropwise and mixed continuously until it changes to a thread-like appearance; at this time, it is poured into the mold and left to cure for 24 hours. Researchers commonly use silicone rubbers such as Ecoflex-30 and RTV-528 for the fabrication of tactile sensors as these materials possess the required mechanical properties (force response) and are biocompatible. The size of the elastomer is Ø 15mm, with a total height of 8 mm. From top to bottom, the total height of the elastomer is distributed as; a 5 mm thick marker, a 1 mm thick solid elastomer layer, and a 2 mm of patterned elastomer layer (posts height).

3.2.3 MRE Marker

The marker, the sensing target in the proposed sensor, is composed of iron particles and the elastomer. The iron particles are added to the elastomer (which is already prepared) in equal volume ratios. The two components are mixed thoroughly until they form a paste-like substance and the mixture has an apparently uniform density (it took 3-4 minutes of continuous mixing). Then the mixture is degassed before being poured into the top cavity of the elastomer and left to cure. There are two types of MREs, i.e., isotropic and anisotropic. The MREs cured under a magnetic field exhibit a chain-like arrangement of particles within the elastomer and are called anisotropic MREs. In our case, no external magnetic field was applied and thus, the particle arrangement was random, forming an isotropic MRE. We did not evaluate the distribution of iron particles in the MRE, but generally, the MREs cured under natural conditions exhibit a uniform distribution of particles. Additionally, the anisotropic MREs offer some limitations like a higher non-linear behavior, a higher loss factor and a strain amplitude softening phenomenon [36], [37]. The content of the iron particles in the literature is reported in either volume fractions

(vol%) or weight fractions (wt.%). The vol% range from 0 to 40% whereas wt.% ranges from 0 to 85% in the literature [38]. We initially prepared MRE samples with different volume ratios (40-60%), but it was observed that increasing the ratio above 50% neither guarantees proper mixing of the two phases nor does the resultant MRE holds the required flexible and soft behaviour. The particle sedimentation problem is reported to occur in liquid-state MREs (MR fluids) only, while solid-state MREs are immune to this phenomenon [36], [39].

3.2.4 Fabrication Process

Molds of Polylactic Acid (PLA) are 3D printed from the university facility for making the elastomer by pouring the mixture into them. As the elastomer has a profile on top and also on the bottom, two separate molds are made and joined together before pouring the mixture into it, as shown in figure 3.4(a). The bottom mold has a cavity of 15 mm diameter with a solid square-shaped center portion of 10 mm × 10 mm area and 5 mm height. After the cure, molds are separated and the elastomer is extracted with care. The cured elastomer has a square-shaped cavity on top and a pattern of posts at the bottom side, as shown in figure 3.4(b). The mixture for the marker is poured into the top cavity of the elastomer and, when cured, becomes part of the elastomer. The marker has the same size as the cavity. A complete elastomer with an MRE marker is shown in figure 3.4(c). The elastomer and the PCB are aligned and fixed together through cyanoacrylate glue. The final assembled sensor is shown in figure 3.4(d). The fabricated sensor has a diameter of 15 mm and a height of 9.6 mm, including PCB thickness. The sensing area is a circle having a diameter of 15 mm, making the sensor symmetric and eligible for an array configuration if required. The initial gap between the marker and PCB is set at 3mm. The actual images of the two prototypes of the proposed sensor after fabrication are shown in figure 3.5.

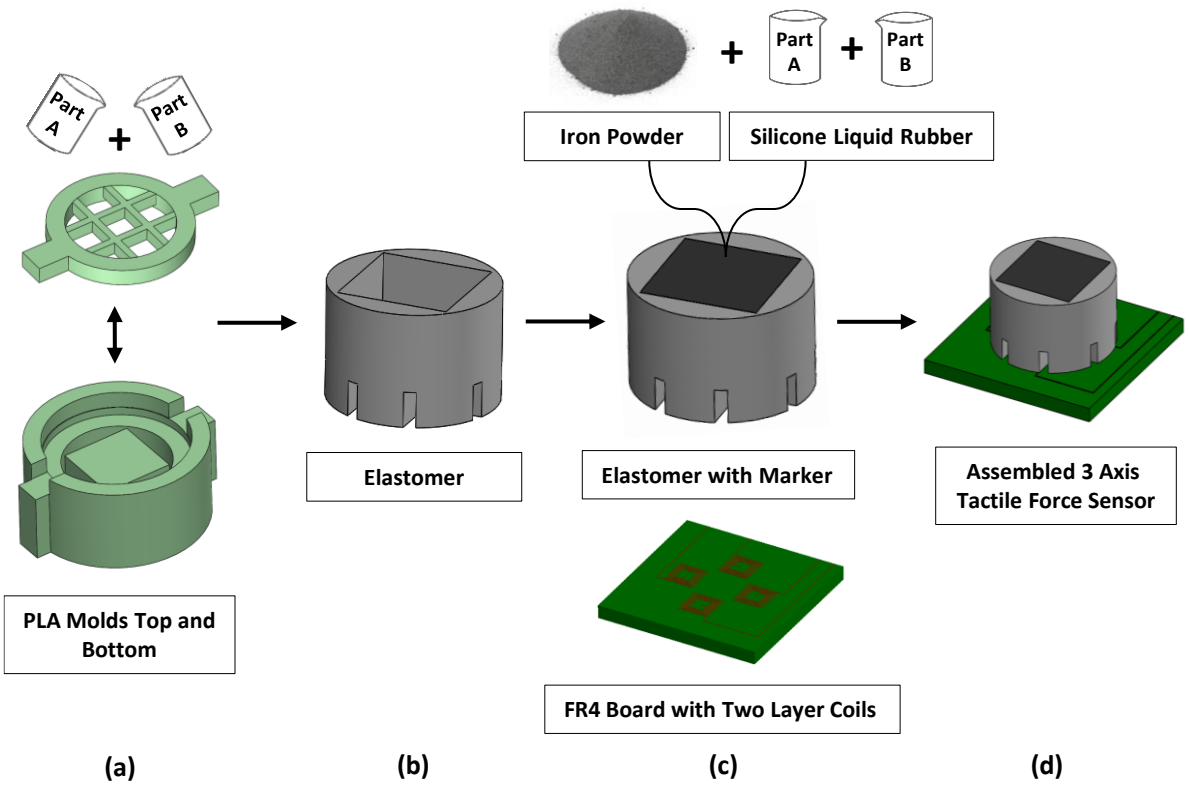

Figure 3. 4 Fabrication stages of the proposed inductive tactile force sensor (a) 3D printed molds for elastomer preparation (b) Ready patterned elastomer (c) Elastomer with marker preparation and fabricated PCB (d) Final assembled sensor.

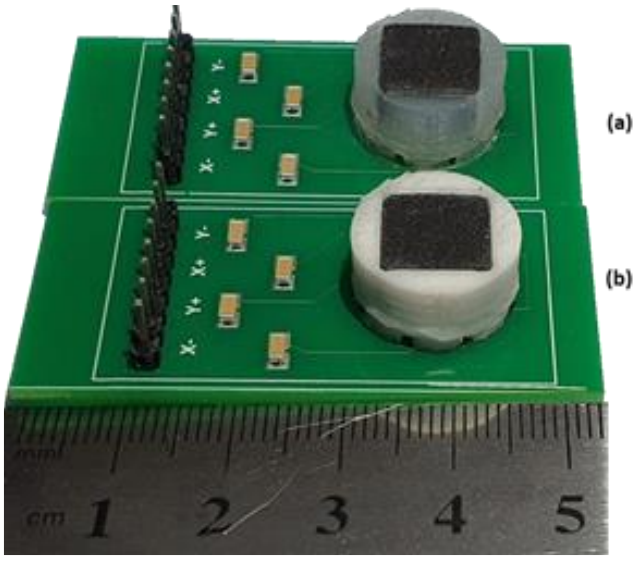

Figure 3. 5 Fabricated sensor with a measurement scale (a) Sensor with Ecoflex-30 elastomer (b) Sensor with RTV-528 elastomer

3.3 Mathematical Modelling

A mathematical model of any system represents a systematic understanding of the system and explains various parameters on which it depends. A model for measuring resultant inductance and corresponding force values is built for the proposed sensor design. The inductance of coils changes with a change in the position of the marker, either the overlapping area of the marker with coils or the distance between them causes it. The model is formed by assuming the movement of the marker is vertical for normal force and horizontal (in-plane) for the shear forces.

3.3.1 Inductance Equations

The four coils in the proposed sensor design give four values of inductances at all times for any kind of input force. The change in these inductance values is considered and combined in a way to give a resultant inductance value in three different axes (X, Y and Z). The inductance of each coil is represented with $L_i (i = 1,2,3,4)$ and its change in inductance with ΔL_i and resultant inductance in each axis with $L_j (j = X, Y \; and \; Z)$. The three equations of resultant inductances are as follows;

$$L_Z = \Delta L_1 + \Delta L_2 + \Delta L_3 + \Delta L_4 \quad (1)$$

$$L_X = \Delta L_4 - \Delta L_3 \quad (2)$$

$$L_Y = \Delta L_1 - \Delta L_2 \quad (3)$$

The above equations are beneficial for differentiating between normal and shear forces and eliminating crosstalk between the axes, giving a pure decoupled desired response. Three cases of input applied forces are discussed to understand the working of the sensor and the corresponding calculations made by the equations.

Normal Force

When a normal force, F_z is applied on the sensor's top, the change detected in the inductance value of all four coils (1,2,3 and 4) is positive due to the gap closing between marker and coils. The change is in nano Henrys (nH). All four values are added together

to give L_Z. L_X and L_Y show insignificant values because ΔL from two of the coils is not present in these equations and the ΔL from other two coils get subtracted (both being positive). Values from all three equations give a very clear signal at the output that the force applied is in the normal direction (Z-axis).

Shear Force in +X-Axis

When a shear force, F_x is applied parallel to the sensor's surface, the change detected in the inductance value of coil 4 is positive and coil 3 is negative, while coil 1 and coil 2 do not show any change in their inductance values (ideally) because the marker still overlaps the same area for coil 1 and coil 2 without exceeding the designed limits and the gap between marker and coil is not changing. L_Z in this case show zero value as ΔL does not change for coil 1 and coil 2 and change of coil 3 and coil 4, one being positive and other being negative, is subtracted (considering equal positive ΔL in coil 4 and negative ΔL in coil 3). L_Y also displays negligible ΔL. L_X is the only parameter that adds the ΔL from coil 4 and coil 3, defining the input force direction in X-axis.

Shear Force in +Y-Axis

When a shear force, F_Y is applied parallel to the surface of the sensor, the change detected in the inductance value of coil 1 is positive and coil 2 is negative, while coil 3 and coil 4 do not show any change in their inductance values. In this case, L_Z show zero value as ΔL does not change for coil 3 and coil 4 and change of coil 1 and coil 2, one being positive and other being negative, is subtracted (considering equal positive ΔL in coil 1 and negative ΔL in coil 2). L_X also displays negligible ΔL. L_Y is the only parameter that adds the ΔL from coil 1 and coil 2, defining the input force direction in Y-axis.

For forces applied in negative x and y-axes, signs of ΔL in equations 2 and 3 will be reversed only.

Angular Forces

The proposed sensor is capable of detecting and distinguishing forces applied in planar angular directions. Four angular forces can be measured, directed towards each quadrant

on a coordinate axis. The resultant inductance value against angular forces can be calculated using the following equations.

$$L_{Q1} = \Delta L_1 + \Delta L_4 - (\Delta L_2 + \Delta L_3) \quad (4)$$

$$L_{Q2} = \Delta L_1 + \Delta L_3 - (\Delta L_2 + \Delta L_4) \quad (5)$$

$$L_{Q3} = \Delta L_2 + \Delta L_3 - (\Delta L_1 + \Delta L_4) \quad (6)$$

$$L_{Q4} = \Delta L_2 + \Delta L_4 - (\Delta L_1 + \Delta L_3) \quad (7)$$

Here L_{Q1}, L_{Q2}, L_{Q3} and L_{Q4} show the inductance change due to an applied force at 45°, 135°, 225° and 315° angles, respectively. The sensor is capable of estimating normal, shear (±X-axis and ±Y-axis) and angular (45°, 135°, 225° and 315°) forces. To measure and isolate these forces, a program can be implemented in a microcontroller to investigate the sequence of changes in ΔL according to Table 3.1 and then apply the respective equations for resultant inductance calculation, which will be used further for force estimation.

3.4 FEM Simulations

3.4.1 Force and Displacement Analysis in ANSYS Workbench

The analysis is performed in ANSYS Workbench software to understand the mechanical behavior of the elastomer material in response to the applied force. As there are two types of elastomers, two different analyses are performed, one with Ecoflex-30 and the other with RTV-528 silicone. Before applying a force in the simulation, the sensor top is covered with a specially designed rigid cover. The rigid covering is made of Polylactic Acid (PLA) or polylactide, a thermoplastic polyester used in 3D printing. The shape of the rigid top is octagonal, which helps in applying all types of forces, uniformly and precisely, for which sensor is designed. The CAD model is made up of four different materials, which are PCB (FR4), elastomer (Ecoflex-30 or RTV-528), MRE marker and

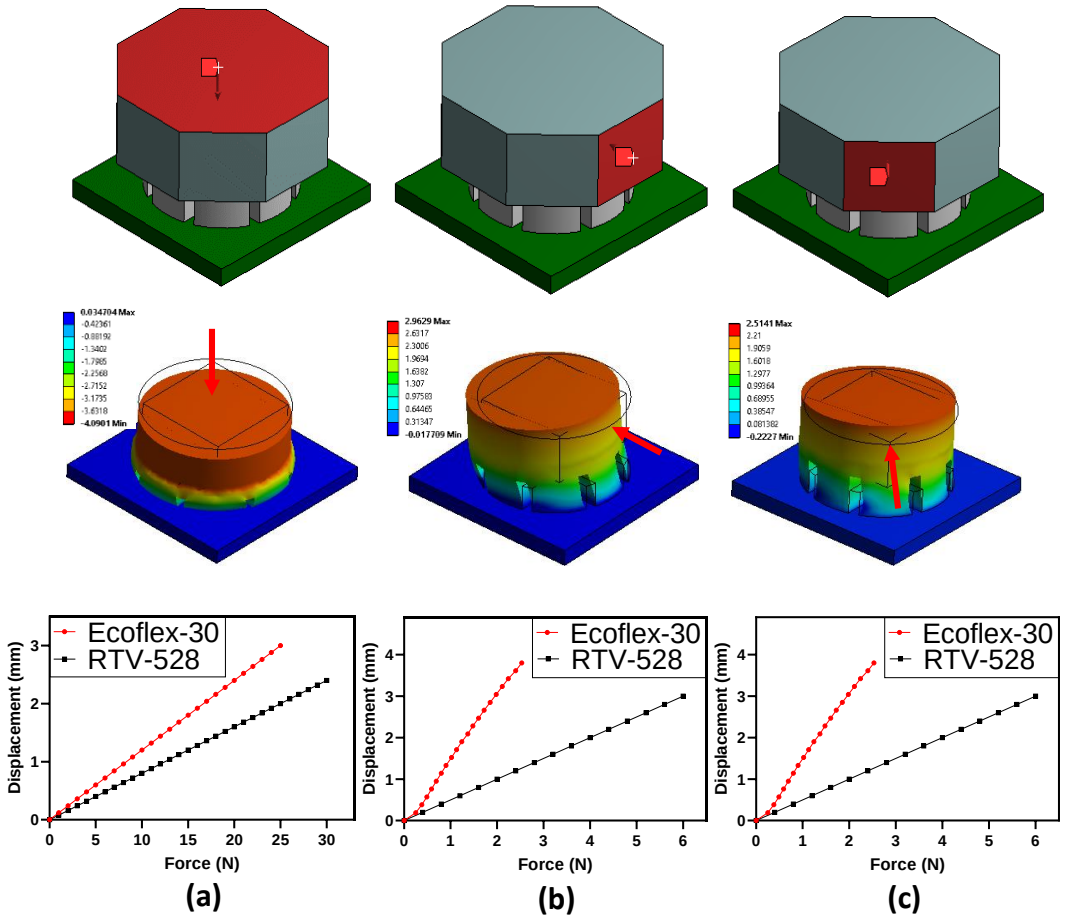

Figure 3. 6 Force displacement analysis in ANSYS Workbench (a) Normal force (b) Shear force (c) Angular force

PLA cover, which are assigned relevant properties required to perform static structural analysis [40-44]. A hyperelastic model named Mooney-Rivlin with parameter values $C_{10} = 0.0096945$ MPa and $C_{10} = 0.0036025$ MPa found from engineering stress-strain curves for Ecoflex-30 presented in [45]. The mechanical behavior of MRE is not investigated due to its complex nature. For the simulation, MRE is also given the properties of the elastomer. The purpose of this simulation is to understand the elastomer's deformation and find the maximum deformation it can withstand for the applied input forces in different directions and study the displacement of its top surface. That is the reason we have not directly compared the simulation and experimental results in the manuscript. The results show that the mechanical displacement sensitivity for Ecoflex-30 is visibly higher than the RTV-528 elastomer as the top surface of the Ecoflex-30 elastomer displaces more in the direction of applied force. The maximum forces are found to be around 30N for normal and 6 N for shear and angular shear forces. The method of

force application, resultant elastomer deformation and performance of two elastomer variants is shown in figure 3.6.

3.4.2 Displacement and Inductance Analysis in ANSYS Maxwell

The magnetic response was necessary for validating the working principle of the proposed sensor design. The magnetostatic analysis is performed in the ANSYS Maxwell to determine the inductance change in the coils by the displacement of the MRE block. A magnetostatic analysis is run in which a simulation environment is set where a CAD model of conductive coils and the marker is imported and placed in a boundary box, as shown in figure 3.7(a). The four dual-layer coils are assigned a copper material, the marker is assigned a ferromagnetic material (iron) and the boundary box as air to contain magnetic field lines originating from the current-carrying coils. The coils are excited by a 1354 mA current going in and out. The coils are assigned a copper material and MRE block is assigned as solid iron as the relevant properties of the MRE, like relative permeability

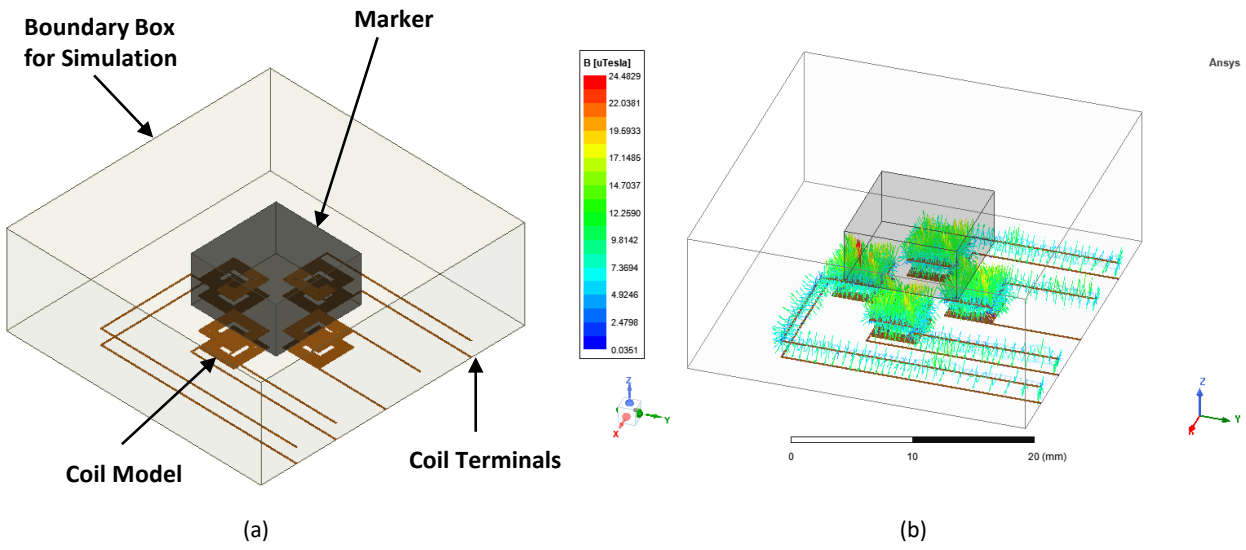

Figure 3. 7 ANSYS Maxwell 3D (a) Simulation environment (b) Magnetic field lines

were not available for the mixture ratio used, and the closest approach to validate the working of the proposed design was to use iron. In this scenario, the simulation results cannot be compared with the experiments, so the inductance values in the simulation

graphs are normalized, focusing only on the response caused by the directional movement of the marker.

To validate the proposed working of the sensor design, the marker is displaced in normal, shear and angular directions and relative inductance changes are plotted as shown in figure 3.8. When the marker is moved vertically down (in -Z-axis), it is observed that the inductance values of all four coils increase exponentially and it is maximum near 3 mm displacement when the marker is closest to the coils. A normalized inductance change is plotted against the displacement as shown in figure 3.8(a). When a displacement is assigned in a shear direction from one extreme to the other (-Y-axis to +Y-axis or from

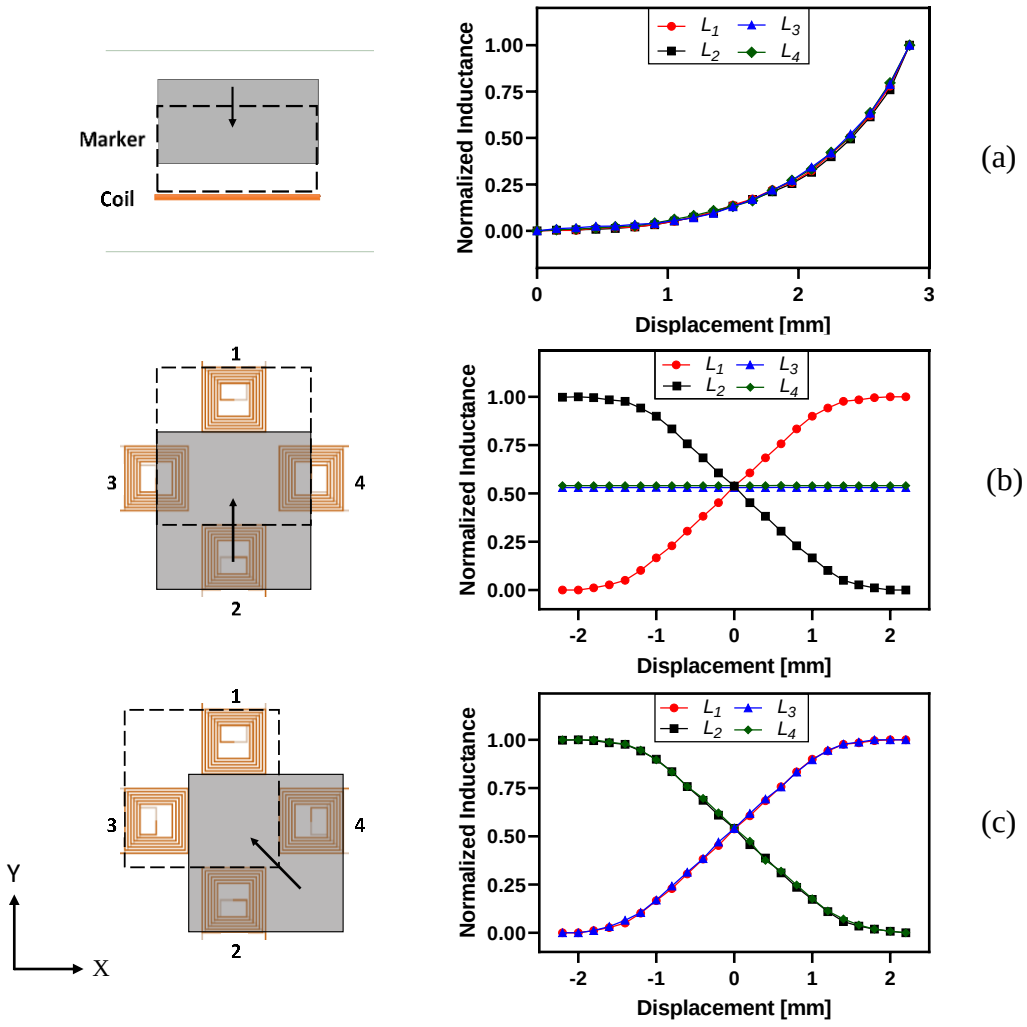

Figure 3. 8 Inductance displacement analysis in ANSYS Maxwell 3D (a) Displacement in –Z axis (b) Shear displacement from –Y-axis to +Y-axis (c) Angular displacement from 4th quadrant to 2nd quadrant.

coil 2 towards coil 1), it is noticed that with an increase in the overlapping area between marker and the coils, inductance increases and vice versa. It is also observed that inductance does not change for coil 3 and coil 4 as the overlapping area for these coils do not change throughout the marker movement path, as shown in figure 3.8(b). Similarly, for an angular movement of the marker from quadrant 4 to quadrant 2, as shown in figure 3.8(c), it is concluded that coil 2 and coil 4 has similar response like coil 1 and coil 3 because the movement of marker is defined in a diagonal path which is a multiple of 45°. This FEM simulation demonstrates the sensor's principle and lays the foundation for the sensor's experimental characterization.

Chapter 4: Experimental Characterization

This chapter provides details about sensor testing in the department's lab. At the start, information about a complete experimental setup and measurement equipment is given. Then, a sequential experimental run for different types of forces and corresponding sensor responses are discussed. After that, a backward force calculation is done, and the results are compared with the calibrated sensor data. Hysteresis and percentage error are calculated and discussed. In the end, several important factors regarding sensor performance and improvement are discussed.

4.1 Experimental Setup

For testing the developed sensor, the Denford Triac-Fanuc CNC milling machine is employed. It is a three-axis machine with two axes (X and Y) moveable stage and one axis (Z) that can move vertically up and down. The displacement resolution for this machine is 1 µm. The sensor is firmly mounted on the stage. A digital push-pull force gauge with a flat tip is mounted on the Z-axis of the machine for applying force to the sensor. The force gauge can detect a minimum force of 10 mN with a force range of up to 50 N. Fore gauge is mounted on a 3D printed fixture which is inserted into the chuck of the CNC machine, it is shown in figure 4.1(a). Two different fixtures are made; one for applying normal force and the other for applying shear and angular forces. The proposed sensor is covered with a rigid cover (plastic indenter) made of PLA material with an octagonal shape. The benefit of using a plastic indenter is to apply uniform force to the sensor in a particular axis. It also keeps the marker in place and does not allow it to stretch or contract while experiencing deformation due to applied force. The plastic indenter has a thickness of 5mm and is glued to the sensor top using cyanoacrylate glue. The two different force application schemes corresponding to normal and shear forces are shown in figure 4.1(b)-(d).

4.2 Measurement and Data Acquisition

The inductance measurement and data acquisition setup are shown in figure 4.2. A four-channel, 28-bit inductance to digital converter evaluation board (LDC1614EVM) from Texas Instruments is attached directly to the proposed sensor. There are four sensing coils (inductors) in the developed sensor each having two terminals connected directly to the board. The evaluation board is connected to the personal computer (PC) through a USB serial interface which also provides power to the board. The board has its own microcontroller and software with a graphical user interface (GUI) for real-time monitoring and data logging. The software continuously monitors the resonance frequency of each attached coil. Each coil has a ceramic non-polar capacitor of 1000 pF capacitance attached in parallel. The capacitor completes the LC circuit and controls the resonance frequency of the circuit. The resonance frequency of each coil sets around 7.0 MHz which is under the 10 MHz limit for the version of the evaluation board used. The inductance value of each coil is calculated by inputting the value of the capacitor in the following equation.

$$f = \frac{1}{2\pi\sqrt{L.(C_{para}+C_{ext})}} \tag{8}$$

Whereas, C_{ext} in the equation is the capacitance of the parallel capacitor and C_{para} is the parasitic capacitance of the interface components and connecting wires. The dual-layer coils printed on the PCB and the connecting wires together have initial inductance values, ranging from 500 nH to 600 nH for each coil. The resonance frequency changes in a way that for a gap closing between marker and the coils or increase in the overlapping area of marker and the coils, it decreases, resulting in an increase in the inductance value according to equation (8).

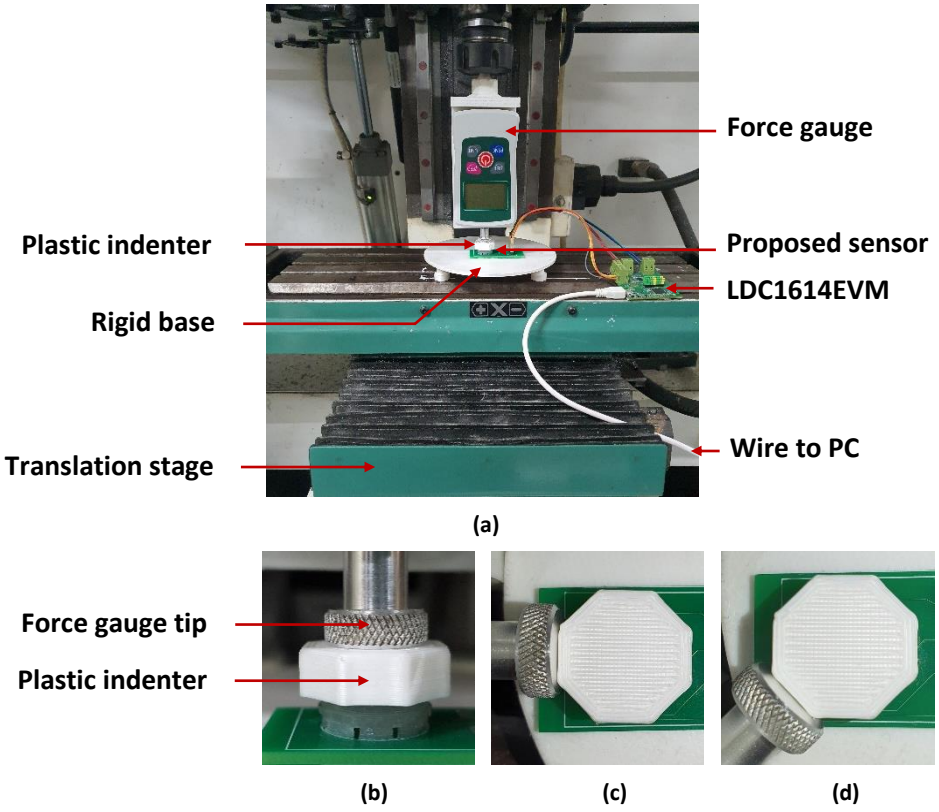

Figure 4. 1 (a) Experimental setup (b) Normal force (c) Shear force and (d) Angular force

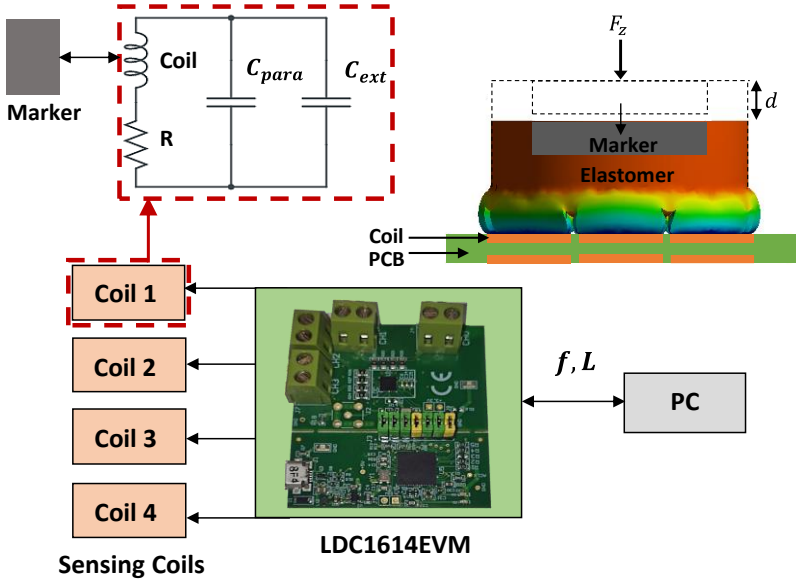

Figure 4. 2 Inductance measurement circuit and electronic interface.

A complete characterization is performed using the apparatus and setup mentioned earlier. When a normal force is applied to the sensor, the Z-axis of the CNC machine is moved downwards such that the gauge's tip barely touches the surface of the plastic indenter to mark the starting point for measurement, as shown in figure 4.1(b). At this point, initial inductance values of the coils are noted from the software. The software is set to log values at a sampling rate of 20 ms. The vertical axis of the CNC machine is manually moved in the -Z-axis at 1 µm displacement, and at regular intervals, the input force value from the LCD of the force gauge and corresponding inductance values from the software are noted. The experiment continues until the inductance values start saturating. For applying shear force in X and Y-axes, the force gauge is mounted horizontally so that the probe faces the side of the plastic indenter, as depicted in figure 4.1(c). In this configuration, the horizontal axis (XY stage) of the machine is moved and respective force values from the gauge and inductance values from the software are noted. For angular force application, the force gauge is rotated to match its tip with the side of the plastic indenter at an angle (say 45°), as represented in figure 4.1(d), and the experiments are repeated in a similar fashion.

4.3 Sensor's Force Response

When a force is applied to the sensor, individual inductances of the four coils and resultant inductances for directional response are found using equation (1)-(7) and plotted against the applied force. Graphs are generated for the proposed sensors made with Ecoflex-30 and RTV-528. Please refer to Appendix A for detailed mathematical model of force response.

4.3.1 Normal Force

When a uniformly distributed normal force is applied to the surface of the proposed sensor, as described in the previous section, the magnetic coupling gets stronger between the sensing coils (inductors) and the sensing target (MRE marker). As a result, the frequency of the inductor circuits decreases, causing an inverse effect in the inductances of the coils. The individual change in the inductances of the coils is shown in figure 4.3, where the inductance change in each coil is different from the other by a small margin but the trend for all four coils is similar, i.e., it increases.

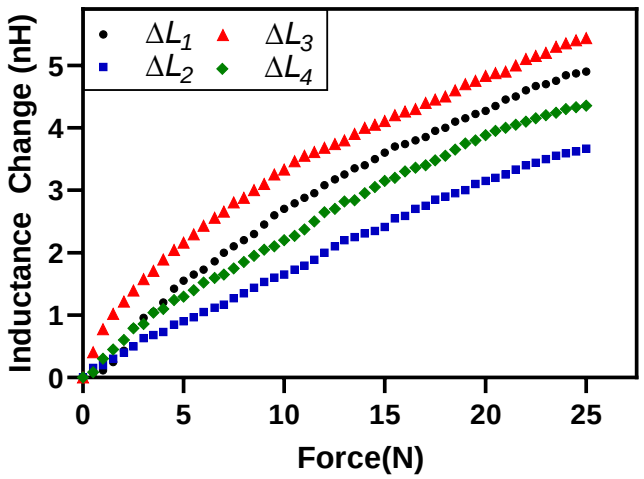

Figure 4. 3 Inductance change in the coils due to normal force

Figure 4.3 corresponds to the response from the sensor made with an Ecoflex-30 elastomer. The response of the sensor made with RTV-528 elastomer is slightly different with the main difference being the less inductance change which can be attributed to the mechanical properties of the elastomer. The non-linear behavior can be understood with the help of equation (8) and simulation results in figure 3.8(a). The equation shows that inductance is related to the frequency as 1/squared powered and figure 3.8(a) also shows that as the marker gets closer to the sensing coils, the increase in inductance of coils becomes exponential in nature.

Figure 4.4 shows the resultant inductance change for an applied normal force calculated using equations (4)-(7). When the sensor experiences force, it compresses and the resultant inductance value (L_z) increases. At the start, the trend is linear, which becomes nonlinear with an increase in the force value as the elastomer compresses. At a point where the elastomer deforms maximum, there is no significant change in the output and the sensor is declared as saturated. It can be seen in the graph that the components of shear forces and angular forces stay close to zero.

The experimental data shows that the sensor made with Ecoflex-30 measures forces up to 25 N with a sensitivity of 0.8 nH/N, whereas the sensor with RTV-528 measures forces up to 30 N at 0.14 nH/N sensitivity. The lesser Young's modulus of Ecoflex-30 allows it to compress easily and possess a higher sensitivity value and RTV-528 elastomer, being

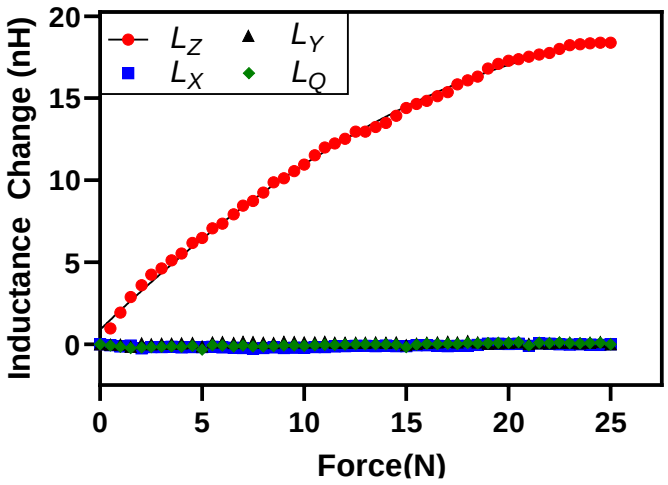

Figure 4. 4 Resultant Inductance for normal force with Ecoflex-30 elastomer

stiffer material, deforms less and offers low sensitivity. The RTV-528 elastomer shows a higher force range due to its ability to offer more resistance to the applied force; its resultant response is presented in Figure 4.5. The output data of L_z in figure 4.4 and figure 4.5 is a curve fitted with a non-linear (second-degree polynomial) trendline using the least squares error approximation method.

4.3.2 Shear Force

When a shear force is applied to the sensor sequentially, as described earlier, the magnetic coupling between the sensing coils and the sensing target changes according to table 3.1, which says that coupling gets stronger in the coil present in the direction of the applied

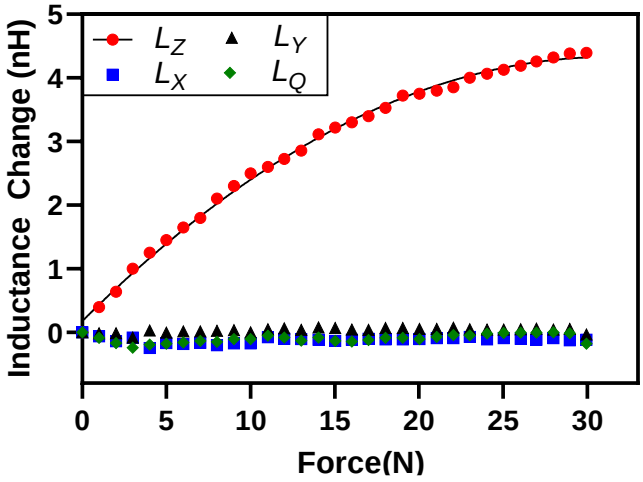

Figure 4. 5 Resultant Inductance for normal force with RTV-528 elastomer

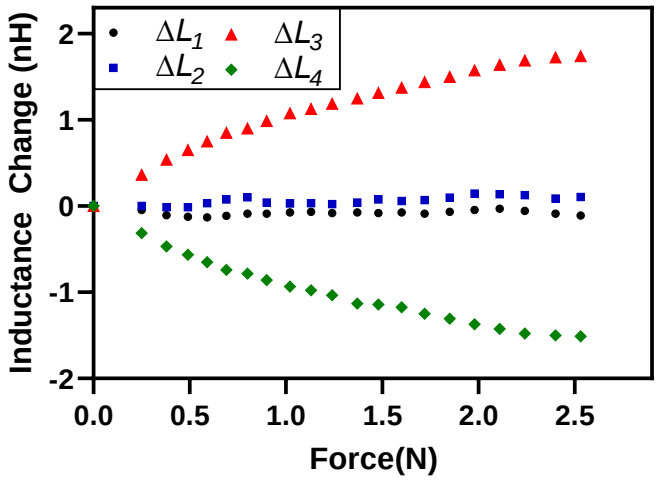

Figure 4. 6 Inductance change in the coils due to shear force

force and decreases in the opposite one whereas for the other two coils it does not change as long as the force is perfectly unidirectional. The individual change in the inductances of the coils is shown in figure 4.6. In this case, force is applied in the -X direction, which, according to the coil configuration proposed in figure 3.1, causes an increase in the inductance value of coil 3 and a decrease in the inductance value of coil 4, whereas minimal changes in the inductances of coil 1 and coil 2 are observed. The non-zero inductance change for coil 1 and coil 2 is due to manufacturing imperfections of the marker where the density of iron particles may vary from one point to another in the whole block of the marker. Figure 4.6 corresponds to the response from the sensor made with an Ecoflex-30 elastomer. The individual inductance changes against an applied shear force for the sensor made with RTV-528 elastomer has a similar response with less inductance change in each coil.

Figure 4.7 shows the resultant accumulated inductance change for the sensor having Ecoflex-30 elastomer for an applied shear force calculated using equations in the mathematical model. The inductance response is linear initially and becomes nonlinear for a high force value, but nonlinearity is quite less as compared to the normal force response. This linear behavior is attributed to the patterned elastomer, which supports marker movement horizontally. There is minor nonlinearity due to the inductance property from equation (8), as discussed earlier. The resultant inductance L_x has a visible response, whereas L_y, L_z and L_Q representing shear, normal and angular resultant inductances have

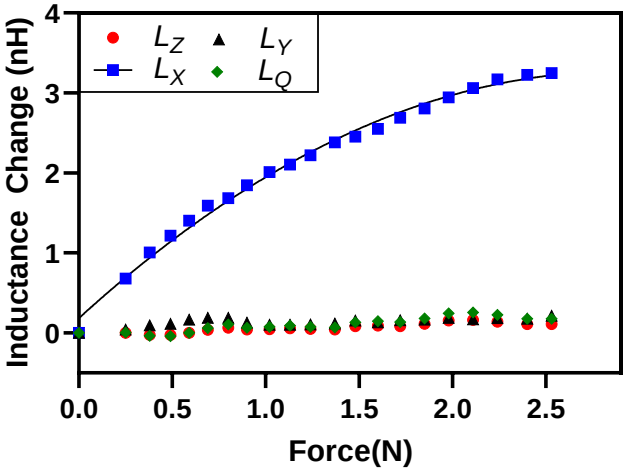

Figure 4. 7 Resultant Inductance for shear force with Ecoflex-30 elastomer

insignificant values. Similar types of resultant inductances are not shown in the graph, as detailed in appendix A to keep the graph simple here. There is a limitation of shear force applied to the sensor, which is defined by the elastomer deformation and hence marker displacement in the shear direction. At rest, the marker overlaps 2.1 mm of each coil (half overlap) which can go to the maximum of 4.2 mm (full overlap) in each direction, giving a maximum overlap and maximum positive inductance change in that direction; this also marks the saturation point of the sensor as design suggests.

The sensor made with Ecoflex-30 elastomer has a range of 2.5 N with a sensitivity of 1.28 nH/N, and the sensor with RTV-528 elastomer has a range of 6 N with a sensitivity of 0.224 nH/N for shear forces. The results in other shear directions (-X-axis and ±Y-axis) are similar due to the symmetric design of the sensor and are not discussed. The shear

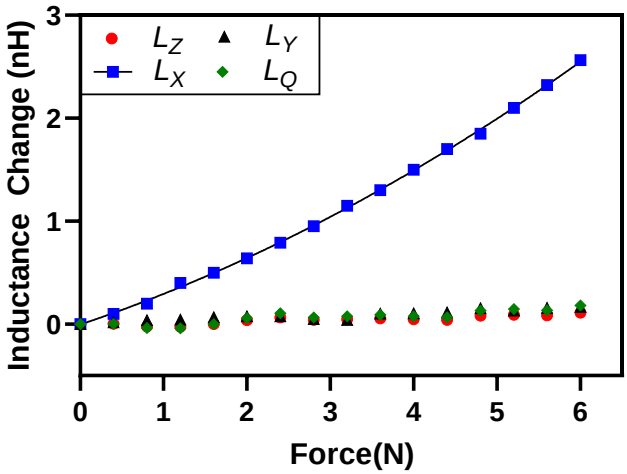

Figure 4. 8 Resultant Inductance for shear force with RTV-528 elastomer

force response for the RTV-528 elastomer is shown in figure 4.8. The responses are curve fitted with a non-linear trend line too.

4.3.3 Angular Force

When an angular force is applied to the sensor, the magnetic coupling of adjacent sensing coils changes with the sensing target; for example, if an angular force is applied at 45°, the inductance values of coil 1 and coil 4 increase as coupling gets stronger whereas the inductance of coil 2 and coil 3 decreases because the marker moves away from these coils. The individual change in the inductances of the coils is shown in figure 4.9 when an angular force is applied at 45°. The response shown is associated with the sensor made

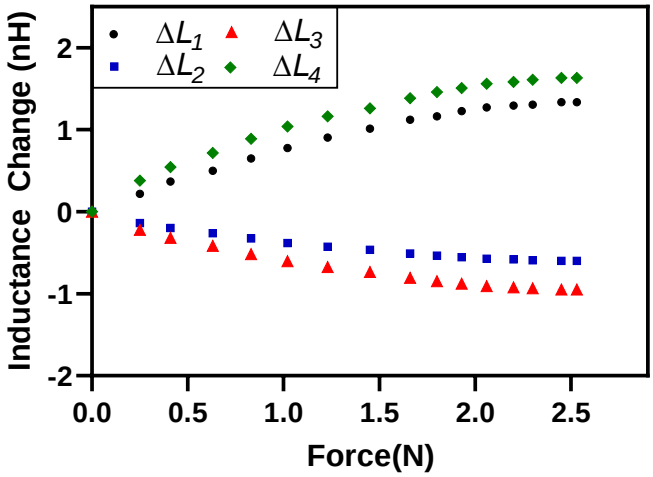

Figure 4. 9 Inductance change in the coils due to angular force

with an Ecoflex-30 elastomer. The individual inductance changes against an applied angular force for the sensor made with RTV-528 elastomer have a similar response with less inductance change value for each coil.

The above sensor response is also supported by the response shown in FEM simulations earlier. The resultant inductance values for an applied angular force at 45° are plotted in figures 4.10 and figure 4.11 for the sensor made with Ecolex-30 and RTV-528 elastomer, respectively. The angular force causes the marker to displace in a diagonal direction, changing individual inductance values of the coils according to Table 3.1 and resultant inductance values by equation (4)-(7). A differential inductance output is formulated to increase the sensitivity and eliminate crosstalk between the axes. The resultant inductance

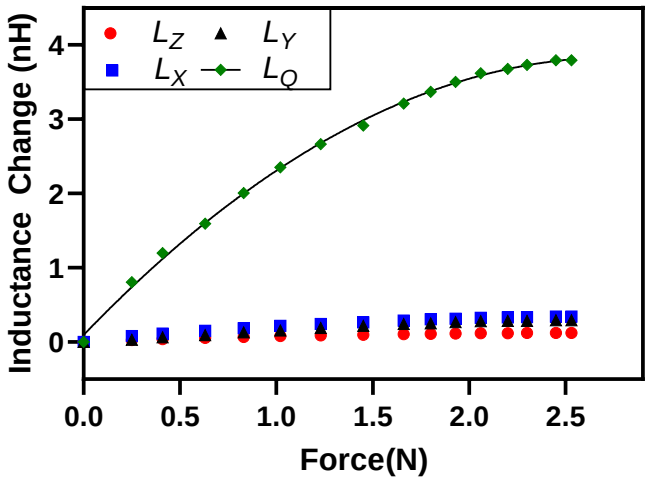

Figure 4. 10 Resultant Inductance for angular force with Ecoflex-30 elastomer

L_Q has a visible response, whereas L_x, L_y and L_z representing normal and shear resultant inductances have insignificant values. The L_Q response shown here belongs to L_{Q1} but for the sake of simplicity, similar types of resultant inductances are not shown in the graph, as detailed in the appendix. A small nonlinearity is observed in the graphs, which is the property of inductance itself, i.e., the inductance increases exponentially with an increasing overlapping area or gap closing. The elastomer displacement in a diagonal direction limits the angular force range. The sensor with Ecoflex-30 is capable of measuring an angular force of 2.5 N with 1.35 nH/N sensitivity, whereas the sensor with RTV-528 elastomer can measure 6 N force with 0.25 nH/N of sensitivity. Angular force responses in other diagonal directions are assumed to be similar. The output data of L_Q in

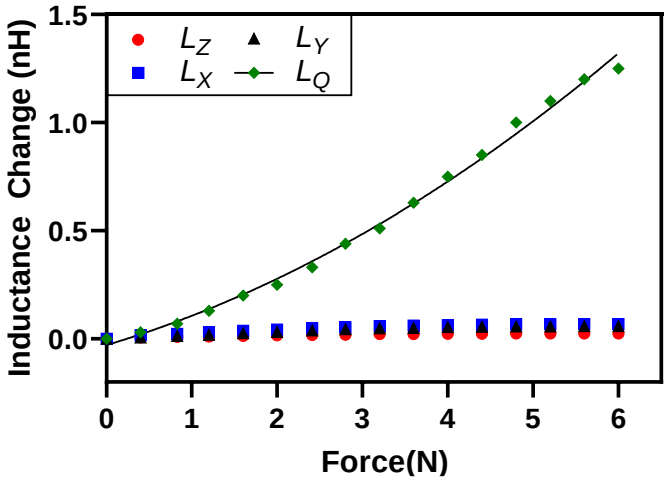

Figure 4. 11 Resultant Inductance for angular force with RTV-528 elastomer

figure 4.10 and figure 4.11 are also curve fitted with a non-linear trendline for understanding the sensor's response and behavior against the applied angular force.

4.4 Hysteresis Calculation

Hysteresis is defined as "the dependence of the state of a system on its history" which defines the behavior of the sensor. A low hysteresis means that the sensor has the same output response for an increasing and decreasing input parameter. A low hysteresis also means that the sensor gets ready for the next input to produce a corresponding output in a minimum time, thus increasing recovery and reaction times. The elastomers used in the proposed sensor prototypes are polymers that are suitable for applications requiring a high dynamic response [46]. The hysteresis error for the proposed inductive tactile force sensor is 7.2% with Ecoflex-30 elastomer and 5.3% with RTV-528 elastomer. The RTV-528 expresses better retentive properties in comparison to Ecoflex-30. The formula used to calculate the hysteresis of the two proposed sensors is given below;

$$\%\ Hysteresis = \frac{maximum\ difference\ between\ loading\ and\ unloading\ value\ of\ inductance}{total\ change\ in\ the\ inductance\ value\ over\ a\ force\ range}\ x\ 100$$

Figure 4.12 and figure 4.13 show the hysteresis for the sensor prototypes made with Ecoflex-30 elastomer and RTV-528 elastomer, respectively. In the hysteresis experimentation, an increasing force is applied at regular intervals on the sensor up to its designed limit and corresponding inductance values are noted down at each point. This is

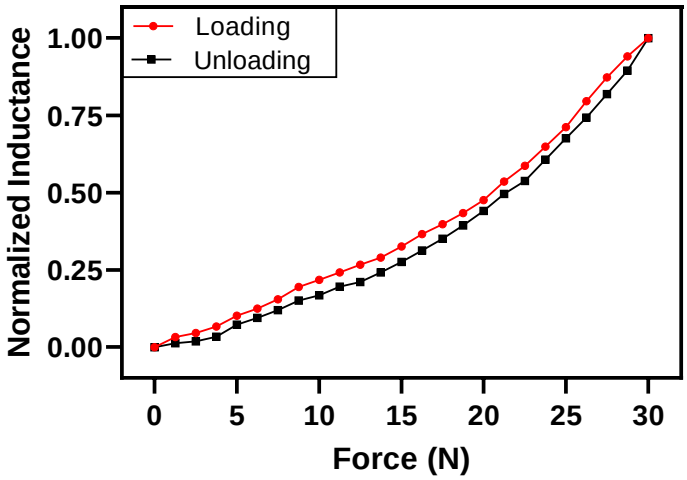

Figure 4. 12 Hysteresis plot of the sensor with RTV-528 elastomer

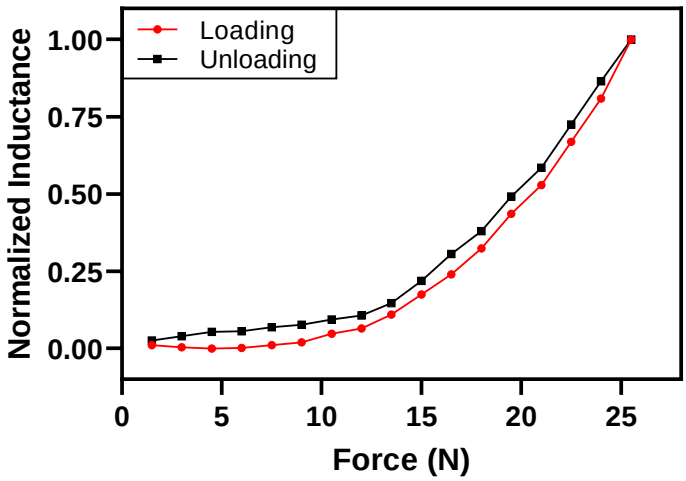

Figure 4. 13 Hysteresis plot of the sensor with Ecofelx-30 elastomer

called a loading phase which is shown as a red line in the graphs. Then, unloading is performed and force is removed from the sensor at the same data points and corresponding inductance values are noted. This is shown as a black line with data points in the graph. A plot is built to visualize the hysteresis. The difference between inductance values during loading and unloading at the same force value is calculated. The maximum difference is kept for further calculation and stays in the numerator of the equation. Also, a difference of maximum and minimum inductance values during the hysteresis is found and goes to the denominator of the equation. The two terms are divided and the result is multiplied by 100 to get a % hysteresis. In graphs, normalized inductance values are used for plotting the results.

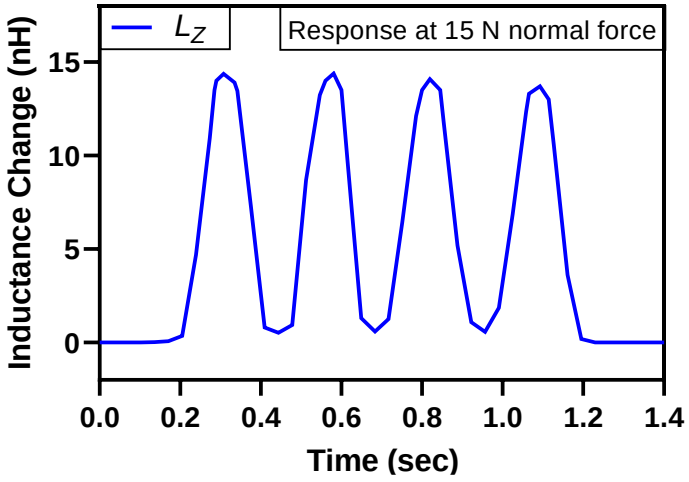

Figure 4. 14 Dynamic response of the proposed sensor

It should be noted that the hysteresis increases at a high force application rate (forcing frequency) and high strain amplitudes [37]. The proposed sensor is designed for a medical application like a minimally invasive surgical procedure which requires a dynamic response up to 3 Hz [47]. The designed sensor is tested for 4 Hz and the response is found suitable for the desired task. The response of the proposed inductive tactile sensor made with Ecoflex-30 at a normal force of 15 N magnitude is shown in figure 4.14.

4.5 Force and Error Estimation

The proposed sensor is calibrated and tested to check its performance. The process starts by applying a known force and noting corresponding inductance values and plotting them, as done in section 4.3. In resultant inductance plots, there are red marks that represent data points where force and inductance value are noted, and there is a solid black line, a trend line generated above these data points to find the data trend. These lines are plotted using a second-order polynomial equation as most of the data has some nonlinearity in it. A general second-order polynomial equation is given below.

$$a_i F_i^2 + b_i F_i + (c_i - \Delta L_i) = 0 \qquad (9)$$

Where ΔL_i is the inductance change of the sensor, F_i is the applied force on the sensor whereas, a_i, b_i, and c_i are the coefficients of the polynomial equation. This process gives the coefficients of the equation (9) and defines a relation between inductance and input force. There is an equation for each of the forces (normal, shear and angular) that the

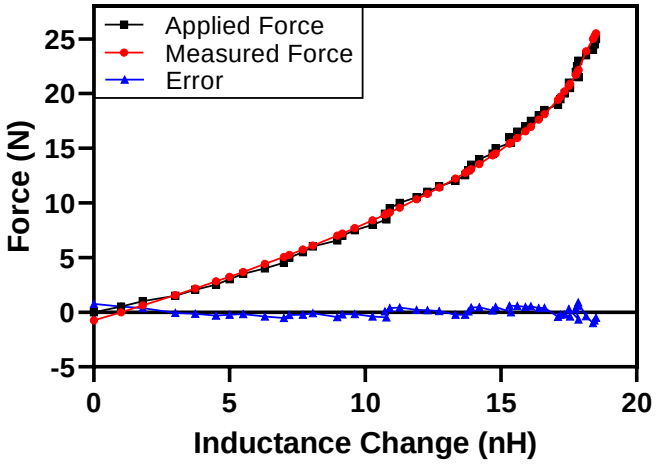

Figure 4. 15 Applied vs measured normal force for Ecoflex-30 elastomer

sensor is capable of measuring. Now, an experiment is performed in which a known *applied force*, corresponding inductance values and a *measured applied force* (calculated by inputting coefficient values from the second-order equation and inductance values in a quadratic formula) are plotted together. This procedure verifies the calibration of the sensor by estimating an error percentage between actual applied force and measured applied force. It also represents the true working and capability of the sensor. Figure 4.15 and figure 4.16 show the known force applied to the sensor, the measured force and the error value between the two, for the sensor made with Ecoflex-30 elastomer. The results for applied normal and shear forces are shown in figure 4.15 and figure 4.16, respectively. It can be seen that the measured force is in close agreement with the applied force to the sensor and the error values are very small, which means that the proposed sensor has a promising performance.

The indentation rate of 0.5 mm/s is used during the experiment for applying the force which is close to the 0.25 mm/s and 1mm/s applied indentation rates in the literature [32-33], [35].

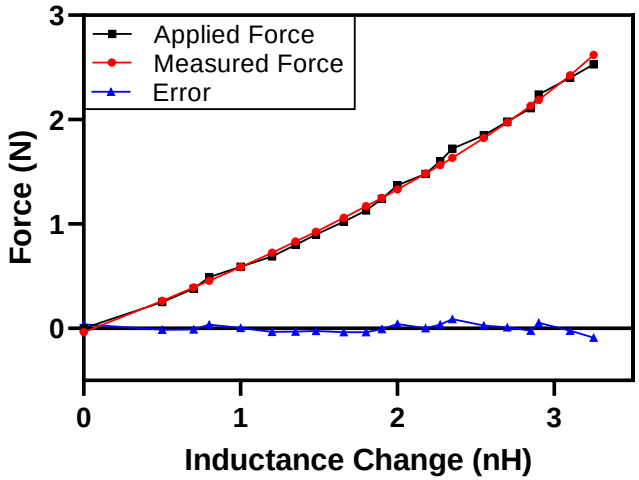

Figure 4. 16 Applied vs measured shear force for Ecoflex-30 elastomer

Chapter 5: Results and Discussion

Table 5.1 presents complete specifications of the developed sensor prototypes. Two prototypes are developed using Ecoflex-30 and RTV-528 silicon rubber as elastomers. They can detect and measure normal, shear and angular forces in multiple directions and can easily differentiate among them using a set of equations. There force range, sensitivity and resolution for each axis is calculated and mentioned in the table given below.

Table 5.1 Characteristics of the proposed sensor prototypes

Force Type	Elastomer Type	Force Range	Sensitivity	Resolution
Normal Force	Ecoflex-30	25 N	0.80 nH/N	12.71 mN
	RTV-528	30 N	0.14 nH/N	76.52 mN
Shear Force (±X and ±Y-axis)	Ecoflex-30	2.5 N	1.28 nH/N	7.96 mN
	RTV-528	6 N	0.22 nH/N	11.70 mN
Shear Angular Force (45°, 135°, 225°, 315°)	Ecoflex-30	2.5 N	1.35 nH/N	6.61 mN
	RTV-528	6 N	0.25 nH/N	23.98 mN

The three-axis inductive sensor based on the MRE marker in the literature reported that the error value between the applied force and the measured force increases as the value of the applied force increases [35]. The reason for this increasing error trend is stated to be the deformation of the marker itself at higher force values. This happens because the fabricated marker is a soft material like the elastomer and for small applied forces, it does not deform but deforms for large forces and does not hold its initial shape. This change in shape causes an increase in an overlapping area of the marker and the underneath coils introduce abnormality in the inductance values. The author used elastomer and iron particles in a 60 to 40 ratio (elastomer: iron particles), which is increased to a 50 to 50

ratio in this work. An MRE with increased iron content causes greater inductance change in the coils, as reported in the literature [48]. Hence, a higher concentration of iron particles is used. MREs with even higher concentrations of iron particles were made initially, such as a 60% volume ratio, but it inhibited proper mixing of the iron particles in the elastomer and the MRE did not remain structurally intact after curing. Thus, a 50% volume ratio of iron particles was adopted because, at this proportion, MRE remained structurally intact and flexible. The increase in iron particles increases the hardness of the MRE marker, making it stiffer enough and hence increasing its resistance to deformation against the applied higher force values. It can be seen in figure 4.16 and figure 4.17 that for a similar range of force values [35], the proposed sensor showed an insignificant error in the measurement.

The performance parameters like sensitivity and resolution of the proposed inductive force sensor depend on the mechanical properties of elastomers used, design of sensing coils and sensing target (marker), and the measurement electronics used. The inductance to digital converter evaluation board, LDC1614EVM, is used to measure the inductance of the coils. The resonance frequency of the LC circuit defines the operating frequency of the LC circuit, which can be tuned by changing the value of the parallel capacitor. A capacitor of 1000 pF capacitance is used, which defines the circuit's resonance frequency and operating frequency as just under 7.0 MHz, which is less than the 10 MHz limit for the inductance measurement board. The measurement board has different frequency resolutions for different resonance frequencies of a circuit. The frequency resolution for a resonance frequency of 7.0 MHz is 71.2 Hz and that defines the minimum detectable inductance change of 10.2 pH [49]. The sensitivity of the proposed sensors is found by noting the inductance change per Newton for each of the applied force directions. The inductance resolution of the measurement board is divided by the sensitivity value of the proposed sensor in a particular direction to find the force resolution of the sensor in that direction.

Another important design aspect of the proposed inductive tactile force sensor is the decoupled force response which eliminates the crosstalk between different axes. A new design configuration of the coils is the foundation of the decoupled response; additionally,

the mathematical equations (1)-(7) are carefully derived to support the same cause. Suppose a standalone working model of the proposed sensor is desired. In that case, the inductance values from the four coils can be given as an input to a microcontroller, and these equations can be implemented in the program, where based on the input applied force, these equations will generate some output which will be further used in equation (8) to estimate the applied force's direction and amplitude.

The purpose of testing two different grades of silicon rubber is to investigate their mechanical behavior keeping in mind the application requirements. One of the sensors is made with Ecoflex-30 and the other with RTV-528. Both of these materials are types of liquid silicone rubbers. The two materials possess different mechanical properties like Young's modulus, density and Poisson's ratio. Due to different properties, elastomers made with these two have different force responses, as discussed in the results section. Both of the elastomers have different stiffness. The elastomer made with Ecoflex-30 is softer than the elastomer made with RTV-528. Due to the difference in the softness, the elastomer made with Ecoflex-30 tends to compress more compared to the elastomer made with RTV-528 for the same amount of applied force. This difference makes the sensor made with Ecoflex-30 elastomer more sensitive with better force measurement resolution and the sensor made with RTV-528 elastomer less sensitive but better suited for high force measurement.

The developed sensors were designed to be used for force feedback in robotic surgical tools. Their size, performance and material properties make them suitable for force feedback if properly integrated with the instruments. The integration into surgical instruments is out of the scope of this research work. There are various surgical specialties which require a different amount of forces to be applied to the tissues during surgical procedures [50]. Table 5.2 shows the types of specialties where these sensors can be employed for force feedback. Additionally, the designed sensors can measure dynamic forces up to 4Hz, which makes them suitable for grasping applications in minimally invasive surgical procedures requiring a frequency of 3 Hz, as discussed in section 4.4.

Table 5.2 Force requirements in different surgical specialties [50]

Category	Mean of Average (N)	Mean of Maximum (N)
General surgery	4.67	11.4
Otorhinolaryngology	8.49	15.6
Obstetrics & gynecology	8.69	10.1
Urology	9.79	15.6

The electromagnetic properties of the MRE (like relative permeability) are not characterized in this work. These properties vary based on the composition of the MRE and require special equipment in order to characterize them [51], [52]. Access to such equipment was not possible. The inductance change simulations are performed using Ansys Maxwell without incorporating the properties of the MRE, instead, a solid iron block in place of MRE is used in the simulations. This magnetic response was necessary for validating the working principle of the proposed sensor design. These simulation results cannot be compared with the experiments, so the inductance values in the simulation graphs are normalized, focusing only on the response caused by the directional movement of the marker.

For sensing the inductance change of the proposed sensors, LDC1614 inductance to digital converter evaluation board by Texas instruments is used. This evaluation board has built-in protections against electromagnetic interference (EMI). Additionally, short-length and twisted pairs of wires are utilized where required. These recommendations were critically adopted to minimize the effect of EMI on the performance of the sensor.

Main Features of the Proposed Tactile Force Sensors

- The inductive tactile sensors [31-33] have a non-flexible contact surface which limits their use as force feedback sensors in robotic surgery.
- The size of the proposed sensors is Ø15 mm × 8 mm, which is four times smaller in the area compared to the MRE-based tactile sensor reported in the literature,

which has a size of Ø30 mm × 10 mm [35]. Also, the force resolutions of the proposed sensors are around 7.96 mN and 12.71 mN for shear (x, y) and normal forces (z-axis), whereas the previously reported MRE-based tactile sensor offers 94.4 mN, 173 mN for x, y and 444 mN for the z-axis.

- A square block of MRE is used, which offers more volume than a cylindrical block of MRE of the same size. The size of the MRE block causes a greater inductance change.
- A patterned elastomer base is introduced in the design, not adopted previously [31-33], [35]. A patterned elastomer base offers less resistance to deformation, making the sensor more sensitive (hence better resolution) for applied forces. It also reduces undesired movement like a tilting of the embedded MRE in the elastomer when shear forces are applied.
- The elastomer volume and the initial gap between the MRE and the sensing coils is reduced to enhance the deformation of elastomer at small forces, making the sensor more responsive.
- A stable and low error value is observed for the range of forces applied to the sensor prototypes.
- In past work, the sensing coils have a 2 × 2 matrix configuration. When a force in the x or y-axis is applied, they get an opposite change in two pairs of coils. They could detect normal and shear forces (x and y-axis), and their mathematical model is designed for it, whereas the proposed configuration of the coils can detect forces in x and y directions, and when a force is applied at an angle in a shear plane, it can also be distinguished as a force in a diagonal direction (45°, 135°, 225° and 315°). This feature increases the sensor's overall sensing capability and provides knowledgeable feedback. Four equations are added to the mathematical model to find the resultant change in the inductance when a shear angular force is experienced.

Table 5.3 Comparison of the prototypes with the inductive tactile force sensors from the literature

	Working Principle	Sensing Area (mm)	Coil Turns	Trace Width & Spacing (μm)	Elastomer Material	Marker Material	Force Range (N)	Sensitivity (nH/N)	Resolution (mN)	Hysteresis (%)
Wang et al. [32]	Inductance change due to eddy current	15 × 15	12	100	Ecoflex-20	Aluminum disc	Normal 13 Shear ±0.7	- 	0.3 (all axes)	-
Wang et al. [33]	Inductance change due to eddy current	15 × 15	12	100	Ecoflex-30	Aluminum disc	Normal (array) 105 Shear (array) ±16	489 nH/mm 494 nH/mm 187 nH/mm	-	5.8
Kawasetsu et al. [35]	Inductance change due to MRE	30 × 30	16	100	Ecoflex-30	Fe powder + Ecoflex-30	Normal 30 Shear ±8	Normal 0.75 Shear 0.75	Normal, 444 Shear *y* 173 Shear *x* 94.4	
This work (Ecoflex-30)	Inductance change due to MRE	15 × 15	6	100	Ecoflex-30	Fe powder + Ecoflex-30	Normal 25 Shear ±2.5 Angle ±2.5	Normal 0.8 Shear 1.28 Angle 1.35	Normal 12.71 Shear 7.96 Angle 6.61	7.2
This work (RTV-528)	Inductance change due to MRE	15 × 15	6	100	Silicone Rubber RTV-528	Fe powder + RTV-528	Normal 30 Shear ±6 Angle ±6	Normal 0.14 Shear 0.224 Angle 0.25	Normal 76.52 Shear 11.70 Angle 23.98	5.3

Conclusion

This research work has proposed a new three-axis inductive tactile force sensor that can be integrated in surgical instruments to measure tool-tissue forces during surgical procedures. A complete design, simulation, fabrication and experimental characterization are discussed. The proposed sensor is made and tested using two different silicone elastomers (Ecoflex-30 and RTV-528) and performance comparison is made between the two. The sensor can measure forces applied to it in multiple directions; normal, shear and angular direction. The size of the sensor is comparable with the sensors from the literature having similar working principles. Complete detail of sensor features, dimensions and comparison between the two proposed prototypes and with the rest of the literature is made in table 5.3. The proposed sensor design addresses the challenges for force feedback integration in surgical tools, as mentioned in the literature. The new features introduced in the proposed design are its new configuration of sensing coils, optimized shape and size of the sensing coils and a patterned elastomer for improving sensitivity and reducing the crosstalk. Other than that, the sensor also measures angular contact forces and has low hysteresis and minimal error values against a standard sensor. In addition to the improved performance and specifications, the exposed area of the sensor is made modular for easy maintenance. The proposed sensor also competes and exceeds the similar type of tactile sensors from the literature. Although, the research with MRE in inductive tactile sensing is currently limited, but will increase over time due to its benefits and the increasing interest of the researchers. This work lays the foundation for future work and advancement for the integration of force feedback in RMIS.

The sensor fabricated with an elastomer made of Ecoflex-30 has a force measurement range of 25 N for normal (Z-axis) and 2.5 N for both shear (±X and ±Y-axes) and angular directions (45°, 135°, 225° and 315°). Ecoflex-30 offers a sensitivity of , 0.8 nH/N for normal, 1.28 nH/N for shear and 1.35 nH/N for angular directions. The minimum detectable force in normal, shear and angular directions are12.71 mN, 7.96 mN and 6.61 mN, respectively.

The sensor fabricated with an elastomer made of RTV-528 has a force measurement range of 30 N for normal (Z-axis) and 6.0 N for both shear (±X and ±Y-axes) and angular

directions (45°, 135°, 225° and 315°). RTV-528 offers a sensitivity of , 0.14 nH/N for normal, 0.224 nH/N for shear and 0.25 nH/N for angular directions. The minimum detectable force in normal, shear and angular directions are 76.52 mN, 11.7 mN and 23.98 mN, respectively.

References

Traditional surgical procedures offer many post-operation disadvantages for patients. Minimally invasive surgery (MIS) offers many health benefits for the patients but bothers the surgeons with fatigue and noisy force feedback. A recent approach is to adopt robot-assisted minimally invasive surgery (RMIS). RMIS is better than traditional and MIS but lacks a force feedback mechanism for the surgeons. Force and tactile feedback are defined and challenges for integration of feedback mechanisms in robotic surgical tools are listed. Different examples of force feedback integrated surgical tools for medical examination and surgical procedures are discussed from the literature. Different transduction mechanisms for force and tactile sensing are also highlighted.

[1] Puangmali, P., Althoefer, K., Seneviratne, L. D., Murphy, D., & Dasgupta, P. (2008). State-of-the-art in force and tactile sensing for minimally invasive surgery. *IEEE Sensors Journal*, *8*(4), 371-381.

[2] *Minimally Invasive Surgery*. (n.d.) [Photograph]. https://media.mehrnews.com/d/2018/12/05/4/2975357.jpg

[3] Uranues, S., Maechler, H., Bergmann, P., Huber, S., Hoebarth, G., Pfeifer, J., ... & Mischinger, H. J. (2002). Early experience with telemanipulative abdominal and cardiac surgery with the Zeus™ Robotic System. *European Surgery*, *34*(3), 190-193.

[4] Guthart, G., & Salisburg, J. (2000). The intuitive telesurgery system: overview and application. W: Proceedings of 2000 IEEE International Conference; 2000, on Robots and Automation. San Francisco, 22-28 april 2000. *IEEE*.

[5] Chioson, F. B., Espiritu, N. M., Munsayac, F. E., Jimenez, F., Lindo, D. E., Santos, M. B., ... & Bugtai, N. T. (2020, December). Recent advancements in robotic minimally invasive surgery: a review from the perspective of robotic surgery in the Philippines. In *2020 IEEE 12th International Conference on Humanoid, Nanotechnology, Information Technology, Communication and Control, Environment, and Management (HNICEM)* (pp. 1-7). IEEE.

[6] *Robotic-surgery*. (n.d.) [Photograph]. https://www.summahealth.org/medicalservices/surgery/about-surgical/robotic-surgery

[7] Tiwana, M. I., Redmond, S. J., & Lovell, N. H. (2012). A review of tactile sensing technologies with applications in biomedical engineering. *Sensors and Actuators A: physical*, *179*, 17-31.

[8] Park, M., Bok, B. G., Ahn, J. H., & Kim, M. S. (2018). Recent advances in tactile sensing technology. *Micromachines*, *9*(7), 321.

[9] Enayati, N., De Momi, E., & Ferrigno, G. (2016). Haptics in robot-assisted surgery: Challenges and benefits. *IEEE reviews in biomedical engineering*, *9*, 49-65.

[10] Talasaz, A., & Patel, R. V. (2012). Integration of force reflection with tactile sensing for minimally invasive robotics-assisted tumor localization. *IEEE Transactions on Haptics*, *6*(2), 217-228.

[11] Feng, A. L., & Song, P. C. (2018). Laryngeal force sensor: quantifying extralaryngeal complications after suspension microlaryngoscopy. *Otolaryngology–Head and Neck Surgery*, *159*(2), 328-334.

[12] Kim, U., Lee, D. H., Yoon, W. J., Hannaford, B., & Choi, H. R. (2015). Force sensor integrated surgical forceps for minimally invasive robotic surgery. *IEEE Transactions on Robotics*, *31*(5), 1214-1224.

[13] Chuang, C. H., Li, T. H., Chou, I. C., & Teng, Y. J. (2016). Piezoelectric tactile sensor for submucosal tumor detection in endoscopy. Sensors and Actuators A: Physical, 244, 299-309.

There are different mechanisms which are adopted for force sensing in the literature. Researchers have worked on capacitive, piezoelectric, piezoresistive, magnetic and inductive mechanisms to introduce tactile force sensing. Examples of the sensors from the medical field using different working principles are discussed in detail. A brief comparison is made of the pros and cons of each mechanism with a focus on the inductive mechanism. The benefits and weaknesses of previously presented inductive tactile force sensors are studied in detail. Finally, the aim and scope of the current research for the design and development of an inductive tactile force sensor is laid out.

[14] J. Fernandes, J. Chen and H. Jiang, "Three-Axis Capacitive Sensor Arrays for Local and Global Shear Force Detection", Journal of Microelectromechanical Systems, vol. 30, no. 5, pp. 799-813, 2021. Available: 10.1109/jmems.2021.3101735

[15] Zhang, Y.R., Jen, Y.H., Mo, C.T., Chen, Y.W., Al-Romaithy, M., Martincic, E. and Lo, C.Y., 2020. "Realization of Multistage Detection Sensitivity and Dynamic Range in Capacitive Tactile Sensors". IEEE Sensors Journal, 20(17), pp.9724-9732.

[16] Chen, Y. L., Xie, J. S., Li, A., Song, F. J., Che, S. R., & Gong, Y. J. (2021). Recognition of Contact Force and Position of a Flexible Array-Less Capacitive Tactile Sensor. IEEE Sensors Journal, 22(1), 130-144.

[17] Ju, F., Wang, Y., Zhang, Z., Wang, Y., Yun, Y., Guo, H., & Chen, B. (2019). A miniature piezoelectric spiral tactile sensor for tissue hardness palpation with catheter robot in minimally invasive surgery. *Smart Materials and Structures*, *28*(2), 025033.

[18] Zhang, Y., Ju, F., Wei, X., Wang, D., & Wang, Y. (2020). A piezoelectric tactile sensor for tissue stiffness detection with arbitrary contact angle. *Sensors*, *20*(22), 6607.

[19] Lin, W., Wang, B., Peng, G., Shan, Y., Hu, H., & Yang, Z. (2021). Skin-inspired piezoelectric tactile sensor array with crosstalk-free row+ column electrodes for spatiotemporally distinguishing diverse stimuli. Advanced Science, 8(3), 2002817.

[20] Takahashi, H., Nakai, A., Thanh-Vinh, N., Matsumoto, K., & Shimoyama, I. (2013). A triaxial tactile sensor without crosstalk using pairs of piezoresistive beams with sidewall doping. *Sensors and Actuators A: Physical*, *199*, 43-48.

[21] Thanh-Vinh, N., Binh-Khiem, N., Takahashi, H., Matsumoto, K., & Shimoyama, I. (2014). High-sensitivity triaxial tactile sensor with elastic microstructures pressing on piezoresistive cantilevers. *Sensors and Actuators A: Physical*, *215*, 167-175.

[22] Lee, D. H., Chuang, C. H., Shaikh, M. O., Dai, Y. S., Wang, S. Y., Wen, Z. H., ... & Pan, C. T. (2021). Flexible Piezoresistive Tactile Sensor Based on Polymeric Nanocomposites with Grid-Type Microstructure. Micromachines, 12(4), 452.

[23] Tomo, T. P., Somlor, S., Schmitz, A., Jamone, L., Huang, W., Kristanto, H., & Sugano, S. (2016). Design and characterization of a three-axis hall effect-based soft skin sensor. *Sensors*, *16*(4), 491.

[24] Tomo, T. P., Schmitz, A., Wong, W. K., Kristanto, H., Somlor, S., Hwang, J., ... & Sugano, S. (2017). Covering a robot fingertip with uSkin: A soft electronic skin with distributed 3-axis force sensitive elements for robot hands. *IEEE Robotics and Automation Letters*, *3*(1), 124-131.

[25] Yan, Y., Hu, Z., Yang, Z., Yuan, W., Song, C., Pan, J., & Shen, Y. (2021). Soft magnetic skin for super-resolution tactile sensing with force self-decoupling. Science Robotics, 6(51), eabc8801.

[26] Fleming, A. J. (2013). A review of nanometer resolution position sensors: Operation and performance. *Sensors and Actuators A: Physical*, *190*, 106-126.

[27] Wang, H., Liu, Y., Li, W., & Feng, Z. (2014, October). Design of ultrastable and high resolution eddy-current displacement sensor system. In *IECON 2014-40th Annual Conference of the IEEE Industrial Electronics Society* (pp. 2333-2339). IEEE.

[28] Wang, H., & Feng, Z. (2013). Ultrastable and highly sensitive eddy current displacement sensor using self-temperature compensation. *Sensors and Actuators A: Physical*, *203*, 362-368.

[29] Wang, H., Li, W., & Feng, Z. (2015). Non-contact thickness measurement of metal films using eddy-current sensors immune to distance variation. *IEEE Transactions on Instrumentation and Measurement*, *64*(9), 2557-2564.

[30] Giesberts, R. B., Sluiter, V. I., & Verkerke, G. J. (2018). Design and test of a new inductive force sensor. *Sensors*, *18*(7), 2079.

[31] Wang, H., Kow, J., Raske, N., De Boer, G., Ghajari, M., Hewson, R., ... & Culmer, P. (2018). Robust and high-performance soft inductive tactile sensors based on the Eddy-current effect. *Sensors and Actuators A: Physical*, *271*, 44-52.

[32] Wang, H., Jones, D., de Boer, G., Kow, J., Beccai, L., Alazmani, A., & Culmer, P. (2018). Design and characterization of tri-axis soft inductive tactile sensors. *IEEE Sensors Journal*, *18*(19), 7793-7801.

[33] Wang, L., Jones, D., Chapman, G. J., Siddle, H. J., Russell, D. A., Alazmani, A., & Culmer, P. (2020). An Inductive Force Sensor for In-Shoe Plantar Normal and Shear Load Measurement. *IEEE Sensors Journal*, *20*(22), 13318-13331.

[34] Chi, C., Sun, X., Xue, N., Li, T., & Liu, C. (2018). Recent progress in technologies for tactile sensors. *Sensors*, *18*(4), 948.

[35] Kawasetsu, T., Horii, T., Ishihara, H., & Asada, M. (2018). Flexible tri-axis tactile sensor using spiral inductor and magnetorheological elastomer. *IEEE Sensors Journal*, *18*(14), 5834-5841.

The design of an inductive tactile force sensor is presented along with schematics and the arrangement of sensing coils. A pattern for inductance variation based on multi-directional forces is formed. Complete specification, design considerations, fabrication methods and optimization approaches related to the sensing coils, elastomer and MRE are discussed with references from the literature. A detailed mathematical model comprising 7 equations for the proposed design based on the inductance changes is presented. Finally, a Finite Element Method (FEM) based simulations are performed to understand the silicon rubber's (elastomer's) mechanical behaviour and validate the MRE's magnetic behaviour. The simulation results are plotted for visualization of the analysis.

[36] Nasir, R. M., Ru, C. F., & Shuib, R. K. (2020, September). State-of-the-art for Magnetorheological Elastomers Fabrication and Hydro-tribological Characterisation. In IOP Conference Series: Materials Science and Engineering (Vol. 920, No. 1, p. 012010). IOP Publishing.

[37] Vatandoost, H., Hemmatian, M., Sedaghati, R., & Rakheja, S. (2020). Dynamic characterization of isotropic and anisotropic magnetorheological elastomers in the oscillatory squeeze mode superimposed on large static pre-strain. Composites Part B: Engineering, 182, 107648.

[38] Bastola, A. K., & Hossain, M. (2020). A review on magneto-mechanical characterizations of magnetorheological elastomers. Composites Part B: Engineering, 200, 108348.

[39] Kang, S. S., Choi, K., Nam, J. D., & Choi, H. J. (2020). Magnetorheological elastomers: Fabrication, characteristics, and applications. Materials, 13(20), 4597.

[40] Mallick, D., Amann, A., & Roy, S. (2014). A nonlinear stretching based electromagnetic energy harvester on FR4 for wideband operation. *Smart Materials and Structures*, *24*(1), 015013.

[41] Park, Y. L., Majidi, C., Kramer, R., Bérard, P., & Wood, R. J. (2010). Hyperelastic pressure sensing with a liquid-embedded elastomer. *Journal of micromechanics and microengineering*, *20*(12), 125029.

[42] Benito, J. A., Jorba, J., Manero, J. M., & Roca, A. (2005). Change of Young's modulus of cold-deformed pure iron in a tensile test. *Metallurgical and Materials Transactions A*, *36*(12), 3317-3324.

[43] Bax, B., & Müssig, J. (2008). Impact and tensile properties of PLA/Cordenka and PLA/flax composites. *Composites science and technology*, *68*(7-8), 1601-1607.

[44] Krautz, M., Werner, D., Schrödner, M., Funk, A., Jantz, A., Popp, J., ... & Waske, A. (2017). Hysteretic behavior of soft magnetic elastomer composites. *Journal of Magnetism and Magnetic Materials*, *426*, 60-63.

[45] Hsu, Y. Y., Lucas, K., Davis, D., Elolampi, B., Ghaffari, R., Rafferty, C., & Dowling, K. (2013). Novel strain relief design for multilayer thin film stretchable interconnects. IEEE Transactions on Electron Devices, 60(7), 2338-2345.

An experimental setup is selected based on the experimental requirements. The hardware includes a CNC milling machine with 3 moveable axes, a commercially available single-axis high-resolution force sensor and a personal computer. The data acquisition system of the proposed sensor consists of an LDC1614 evaluation board and software from Texas Instruments (TI). Different forces (normal, shear and shear angle) are applied to the proposed sensor prototypes one at a time, and their response is noted. Experimental data is curve fitted with a second-order polynomial equation, and a force estimation is done. An experiment is also performed to check the hysteresis of the sensor. Also, the dynamic response of the sensor for the designed limit according to a surgical application is carried out.

[46] Hsu, Y. Y., Lucas, K., Davis, D., Elolampi, B., Ghaffari, R., Rafferty, C., & Dowling, K. (2013). Novel strain relief design for multilayer thin film stretchable interconnects. *IEEE Transactions on Electron Devices*, *60*(7), 2338-2345.

[47] Sarmah, A., & Gulhane, U. D. (2010, December). Surgical robot teleoperated laparoscopic grasper with haptics feedback system. In INTERACT-2010 (pp. 288-291). IEEE.

The results from experiments are summarized with complete specifications (force range, sensitivity and resolution) of the proposed sensor prototypes. Different optimisation aspects of removing cross-talk related to MRE mixture ratio and elastomer shape and design are discussed. The application of the proposed sensor is defended according to the force ranges required in multiple surgeries, as mentioned in the literature. Complete specifications of the sensor design are summarized with future recommendations. A comparison is made with the state-of-the-art inductive tactile force sensors from the literature. In the end, a conclusion to this research work is presented.

[48] Wu, C., Cheng, C., Abd El-Aty, A., Li, T., Qin, Y., Yang, Q., ... & Guo, X. (2020). Influence of particles size and concentration of carbonyl iron powder on magnetorheological properties of silicone rubber-based magnetorheological elastomer. Materials Research Express, 7(8), 086101.

[49] *Texas Instruments*. LDC1614 Evaluation Module for Inductance to Digital Converter. https://www.ti.com/tool/LDC1614EVM

[50] *Golahmadi, A. K., Khan, D. Z., Mylonas, G. P., & Marcus, H. J. (2021). Tool-tissue forces* in surgery: A systematic review. *Annals of Medicine and Surgery*, *65*, 102268.

[51] Perales-Martínez, I. A., Palacios-Pineda, L. M., Lozano-Sánchez, L. M., Martínez-Romero, O., Puente-Cordova, J. G., & Elías-Zúñiga, A. (2017). Enhancement of a magnetorheological PDMS elastomer with carbonyl iron particles. Polymer Testing, 57, 78-86.

[52] Lokander, M., & Stenberg, B. (2003). Performance of isotropic magnetorheological rubber materials. Polymer Testing, 22(3), 245-251.

Appendices

Appendix A: Detailed Mathematical Model

To implement the proposed mathematical model of the developed sensor in an actual test environment, a microcontroller programmed with the complete set of equations is recommended. The equations (1)-(7) work well for differentiating forces in normal and positive shear directions without considering the effect in negative directions and interference of shear and angular forces for each other. For that, detailed equations are developed and verified using experimental data. The sensor's response is established using the set of equations mentioned here and is found to be completely decoupled, as shown in the graphs in section 4.3.

In total, the proposed sensor design can differentiate nine different types of input forces. A conditional statement can be used to identify the direction of the applied force, and a corresponding set of equations can be implemented to find the resultant inductance and then this information can be used in the calibrated equation of a particular axis to find out the magnitude of the force in that direction.

I. Equations of resultant inductances for Normal Force calculation

$$L_z = \Delta L_1 + \Delta L_2 + \Delta L_3 + \Delta L_4$$
$$L_{x+} = \Delta L_4 - \Delta L_3$$
$$L_{x-} = \Delta L_3 - \Delta L_4$$
$$L_{y+} = \Delta L_1 - \Delta L_2$$
$$L_{y-} = \Delta L_2 - \Delta L_1$$
$$L_{Q1} = \Delta L_1 + \Delta L_4 - (\Delta L_2 + \Delta L_3)$$
$$L_{Q2} = \Delta L_1 + \Delta L_3 - (\Delta L_2 + \Delta L_4)$$
$$L_{Q3} = \Delta L_2 + \Delta L_3 - (\Delta L_1 + \Delta L_4)$$
$$L_{Q4} = \Delta L_2 + \Delta L_4 - (\Delta L_1 + \Delta L_3)$$

II. Equations of resultant inductances for Shear Force calculation (X+)

$$L_z = \Delta L_1 + \Delta L_2 + \Delta L_3 + \Delta L_4$$
$$L_{x+} = \Delta L_4 - \Delta L_3$$
$$L_{x-} = \Delta L_3 + \Delta L_4$$
$$L_{y+} = \Delta L_1 - \Delta L_2$$

$$L_{y-} = \Delta L_2 - \Delta L_1$$
$$L_{Q1} = \Delta L_1 + \Delta L_4 + (\Delta L_2 + \Delta L_3)$$
$$L_{Q2} = \Delta L_1 + \Delta L_3 + (\Delta L_2 + \Delta L_4)$$
$$L_{Q3} = \Delta L_2 + \Delta L_3 + (\Delta L_1 + \Delta L_4)$$
$$L_{Q4} = \Delta L_2 + \Delta L_4 + (\Delta L_1 + \Delta L_3)$$

III. Equations of resultant inductances for Shear Force calculation (X-)

$$L_z = \Delta L_1 + \Delta L_2 + \Delta L_3 + \Delta L_4$$
$$L_{x+} = \Delta L_4 + \Delta L_3$$
$$L_{x-} = \Delta L_3 + \Delta L_4$$
$$L_{y+} = \Delta L_1 - \Delta L_2$$
$$L_{y-} = \Delta L_2 - \Delta L_1$$
$$L_{Q1} = \Delta L_1 + \Delta L_4 + (\Delta L_2 + \Delta L_3)$$
$$L_{Q2} = \Delta L_1 + \Delta L_3 + (\Delta L_2 + \Delta L_4)$$
$$L_{Q3} = \Delta L_2 + \Delta L_3 + (\Delta L_1 + \Delta L_4)$$
$$L_{Q4} = \Delta L_2 + \Delta L_4 + (\Delta L_1 + \Delta L_3)$$

IV. Equations of resultant inductances for Shear Force calculation (Y+)

$$L_z = \Delta L_1 + \Delta L_2 + \Delta L_3 + \Delta L_4$$
$$L_{x+} = \Delta L_4 - \Delta L_3$$
$$L_{x-} = \Delta L_3 - \Delta L_4$$
$$L_{y+} = \Delta L_1 - \Delta L_2$$
$$L_{y-} = \Delta L_2 + \Delta L_1$$
$$L_{Q1} = \Delta L_1 + \Delta L_4 + (\Delta L_2 + \Delta L_3)$$
$$L_{Q2} = \Delta L_1 + \Delta L_3 + (\Delta L_2 + \Delta L_4)$$
$$L_{Q3} = \Delta L_2 + \Delta L_3 + (\Delta L_1 + \Delta L_4)$$
$$L_{Q4} = \Delta L_2 + \Delta L_4 + (\Delta L_1 + \Delta L_3)$$

V. Equations of resultant inductances for Shear Force calculation (Y-)

$$L_z = \Delta L_1 + \Delta L_2 + \Delta L_3 + \Delta L_4$$
$$L_{x+} = \Delta L_4 - \Delta L_3$$
$$L_{x-} = \Delta L_3 - \Delta L_4$$
$$L_{y+} = \Delta L_1 + \Delta L_2$$
$$L_{y-} = \Delta L_2 - \Delta L_1$$
$$L_{Q1} = \Delta L_1 + \Delta L_4 + (\Delta L_2 + \Delta L_3)$$
$$L_{Q2} = \Delta L_1 + \Delta L_3 + (\Delta L_2 + \Delta L_4)$$
$$L_{Q3} = \Delta L_2 + \Delta L_3 + (\Delta L_1 + \Delta L_4)$$
$$L_{Q4} = \Delta L_2 + \Delta L_4 + (\Delta L_1 + \Delta L_3)$$

VI. Equations of resultant inductances for Angular Force calculation (45°)

$$L_z = \Delta L_1 + \Delta L_2 + \Delta L_3 + \Delta L_4$$
$$L_{x+} = \Delta L_4 + \Delta L_3$$
$$L_{x-} = \Delta L_3 - \Delta L_4$$
$$L_{y+} = \Delta L_1 + \Delta L_2$$
$$L_{y-} = \Delta L_2 + \Delta L_1$$
$$L_{Q1} = \Delta L_1 + \Delta L_4 - (\Delta L_2 + \Delta L_3)$$
$$L_{Q2} = \Delta L_1 + \Delta L_3 - (\Delta L_2 + \Delta L_4)$$
$$L_{Q3} = \Delta L_2 + \Delta L_3 + (\Delta L_1 + \Delta L_4)$$
$$L_{Q4} = \Delta L_2 + \Delta L_4 - (\Delta L_1 + \Delta L_3)$$

VII. Equations of resultant inductances for Angular Force calculation (135°)

$$L_z = \Delta L_1 + \Delta L_2 + \Delta L_3 + \Delta L_4$$
$$L_{x+} = \Delta L_4 + \Delta L_3$$
$$L_{x-} = \Delta L_3 - \Delta L_4$$
$$L_{y+} = \Delta L_1 + \Delta L_2$$
$$L_{y-} = \Delta L_2 + \Delta L_1$$
$$L_{Q1} = \Delta L_1 + \Delta L_4 - (\Delta L_2 + \Delta L_3)$$
$$L_{Q2} = \Delta L_1 + \Delta L_3 - (\Delta L_2 + \Delta L_4)$$
$$L_{Q3} = \Delta L_2 + \Delta L_3 + (\Delta L_1 + \Delta L_4)$$
$$L_{Q4} = \Delta L_2 + \Delta L_4 + (\Delta L_1 + \Delta L_3)$$

VIII. Equations of resultant inductances for Angular Force calculation (225°)

$$L_z = \Delta L_1 + \Delta L_2 + \Delta L_3 + \Delta L_4$$
$$L_{x+} = \Delta L_4 + \Delta L_3$$
$$L_{x-} = \Delta L_3 - \Delta L_4$$
$$L_{y+} = \Delta L_1 + \Delta L_2$$
$$L_{y-} = \Delta L_2 + \Delta L_1$$
$$L_{Q1} = \Delta L_1 + \Delta L_4 + (\Delta L_2 + \Delta L_3)$$
$$L_{Q2} = \Delta L_1 + \Delta L_3 - (\Delta L_2 + \Delta L_4)$$
$$L_{Q3} = \Delta L_2 + \Delta L_3 - (\Delta L_1 + \Delta L_4)$$
$$L_{Q4} = \Delta L_2 + \Delta L_4 + (\Delta L_1 + \Delta L_3)$$

IX. Equations of resultant inductances for Angular Force calculation (315°)

$$L_z = \Delta L_1 + \Delta L_2 + \Delta L_3 + \Delta L_4$$
$$L_{x+} = \Delta L_4 + \Delta L_3$$
$$L_{x-} = \Delta L_3 - \Delta L_4$$
$$L_{y+} = \Delta L_1 + \Delta L_2$$
$$L_{y-} = \Delta L_2 + \Delta L_1$$

$$L_{Q1} = \Delta L_1 + \Delta L_4 + (\Delta L_2 + \Delta L_3)$$
$$L_{Q2} = \Delta L_1 + \Delta L_3 + (\Delta L_2 + \Delta L_4)$$
$$L_{Q3} = \Delta L_2 + \Delta L_3 - (\Delta L_1 + \Delta L_4)$$
$$L_{Q4} = \Delta L_2 + \Delta L_4 - (\Delta L_1 + \Delta L_3)$$

Appendix B: Configuration of the Software

This appendix provides a tutorial for configuring a "Sensing Solutions EVM GUI" for the LDC1614 evaluation module from Texas Instruments.

I. Configuration Page

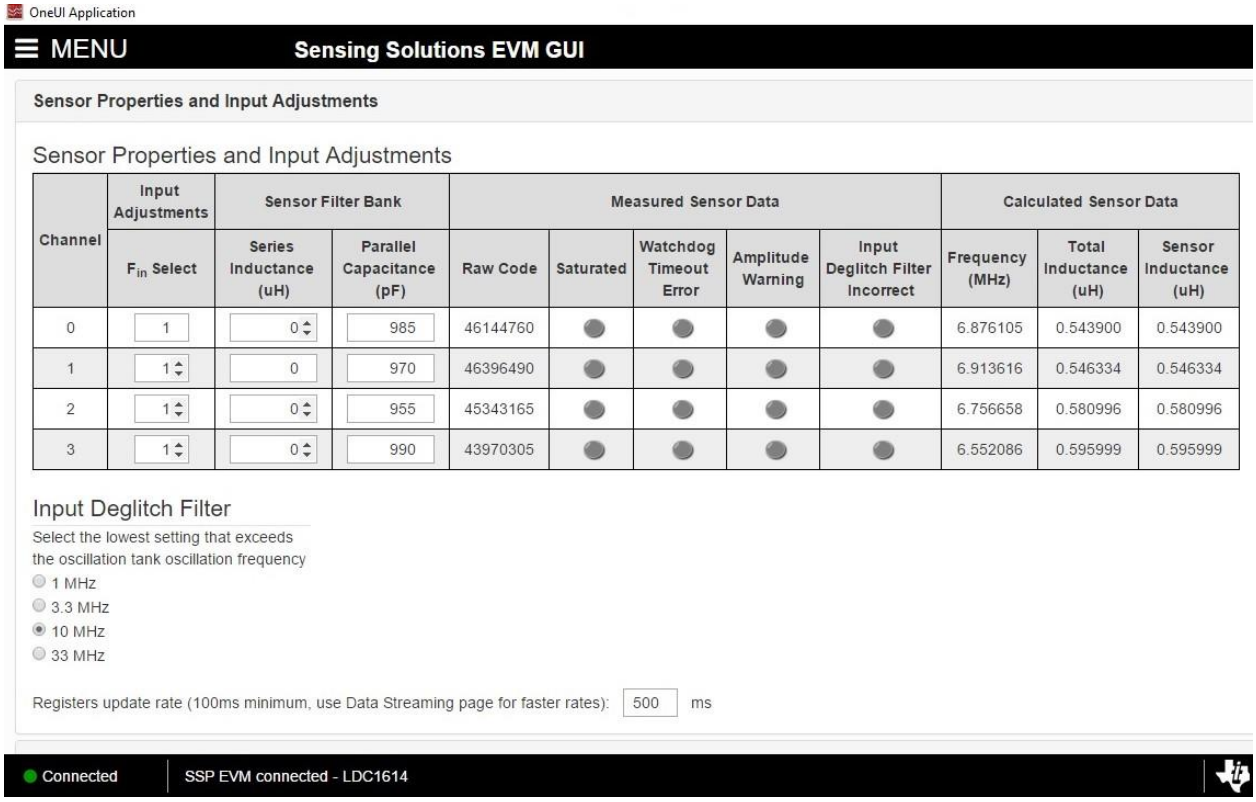

Channel	Input Adjustments	Sensor Filter Bank		Measured Sensor Data					Calculated Sensor Data		
	F_{in} Select	Series Inductance (uH)	Parallel Capacitance (pF)	Raw Code	Saturated	Watchdog Timeout Error	Amplitude Warning	Input Deglitch Filter Incorrect	Frequency (MHz)	Total Inductance (uH)	Sensor Inductance (uH)
0	1	0	985	46144760					6.876105	0.543900	0.543900
1	1	0	970	46396490					6.913616	0.546334	0.546334
2	1	0	955	45343165					6.756658	0.580996	0.580996
3	1	0	990	43970305					6.552086	0.595999	0.595999

- If there is a red indicator in the measured sensor data tab in front of any channel entry, that means loose wiring exists for that channel.
- The evaluation module outputs the raw code in the form of frequency (MHz) and a user is required to input the capacitance of the parallel capacitor installed (pF), which is used to calculate the total inductance (μH) of each inductor.

- The maximum value of the input deglitch filter for the model of LDC used is 10 MHz. The selected option is always higher than the frequency of the LC circuits attached.

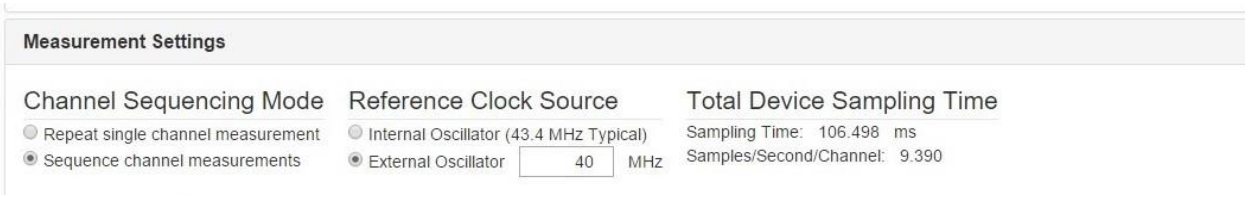

- The "sequence channel measurements" option ensures reading across all channels.
- Select an external oscillator and write 40 MHz in the box. This oscillator is available on the EVM itself.

Measurement Timings

Channel	Enable	F_{ref}		Settle Count		Reference Count		Timing		$ENOB_{max}$
		Divider Code	Calculated (MHz)	Code	Time (us)	Code	Time (us)	Switching (us)	Sampling (us)	
0	☑	1	40.000	1024	409.60	65535	26214.10	0.81600	26624.52	21.0
1	☑	1	40.000	1024	409.60	65535	26214.10	0.81600	26624.52	21.0
2	☑	1	40.000	1024	409.60	65535	26214.10	0.81600	26624.52	21.0
3	☑	1	40.000	1024	409.60	65535	26214.10	0.81600	26624.52	21.0

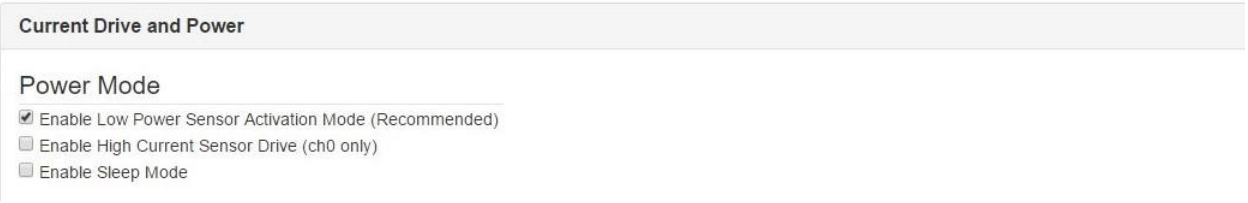

- To enable different channels, mark the relevant check box so that the EVM starts communicating with them. The rest of the settings can be changed if required.

Sensor Initialization Current

Channel	I_{drive}		Detect I_{drive} Init	
	Code	Current (uA)	Code	Current (uA)
0	17	196	30	1354
1	17	196	30	1354
2	17	196	30	1354
3	17	196	30	1354

- After wiring up the circuit and checking for any discontinuity, click on "Detect I_{drive} init" tab to find out the current in the LC circuits and copy its code to the code column in I_{drive} tab. For example, the code for 1354 µA current is 30, which is required to enter in the I_{drive} code column.

II. Data Streaming

- The data streaming page is shown below. It has a graphical area where real-time data can be seen. To start streaming data on the plot, check relevant channels and click the start button. Similarly, a stop button is used to stop the data stream.
- Three different types of output data, inductance, raw code and detected sensor frequency (of LC circuits), can be displayed on the plot, one at a time.
- The graph displays data from all four channels using a different color code.
- Graph settings and statistics are also available on this page.
- A log file (excel file) can be selected or created to log the data while the data stream is turned on.

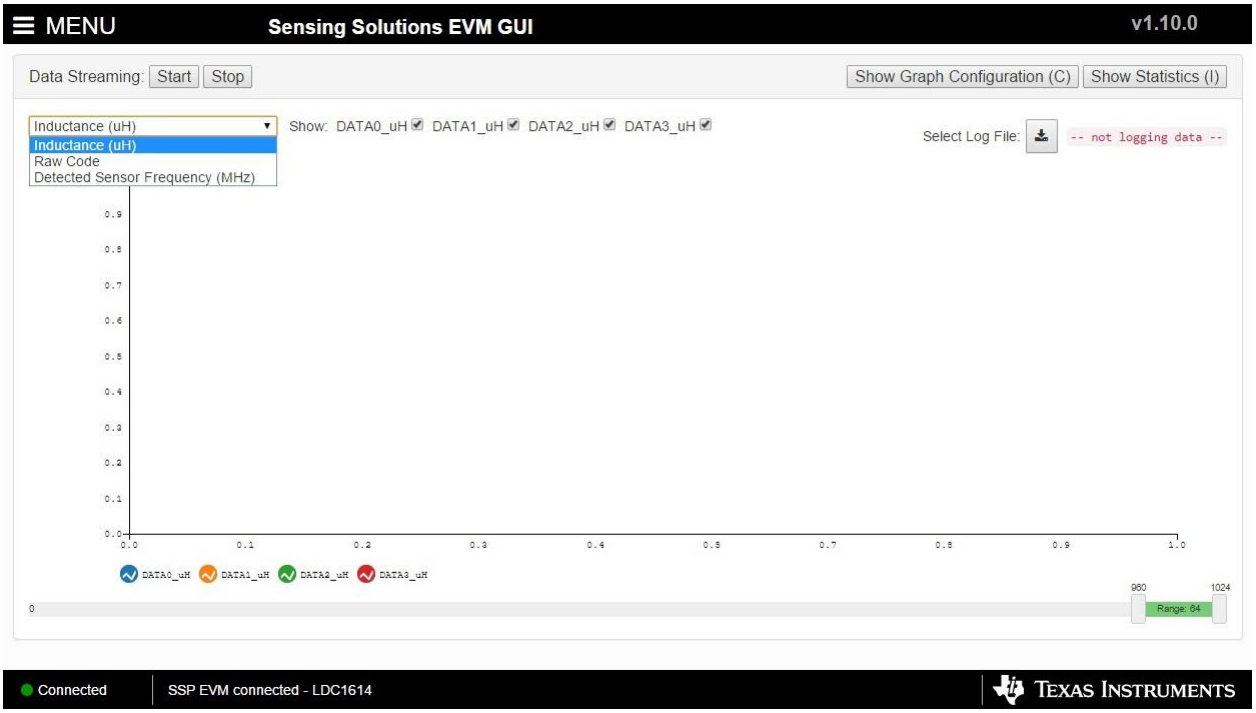

- Clicking the "show graph configuration" button displays the settings panel where a sampling time can be set, which defines the frequency of the sampling. This affects the amount of data generated and logged. Other than sampling settings, the axes of the graph can be adjusted for preferred visualization.

- Statistics show data from all channels based on the type of data selected for streaming. Current values, average values or other variations can be selected based on the application requirement. Decimals can be added as well for observation of minute changes.

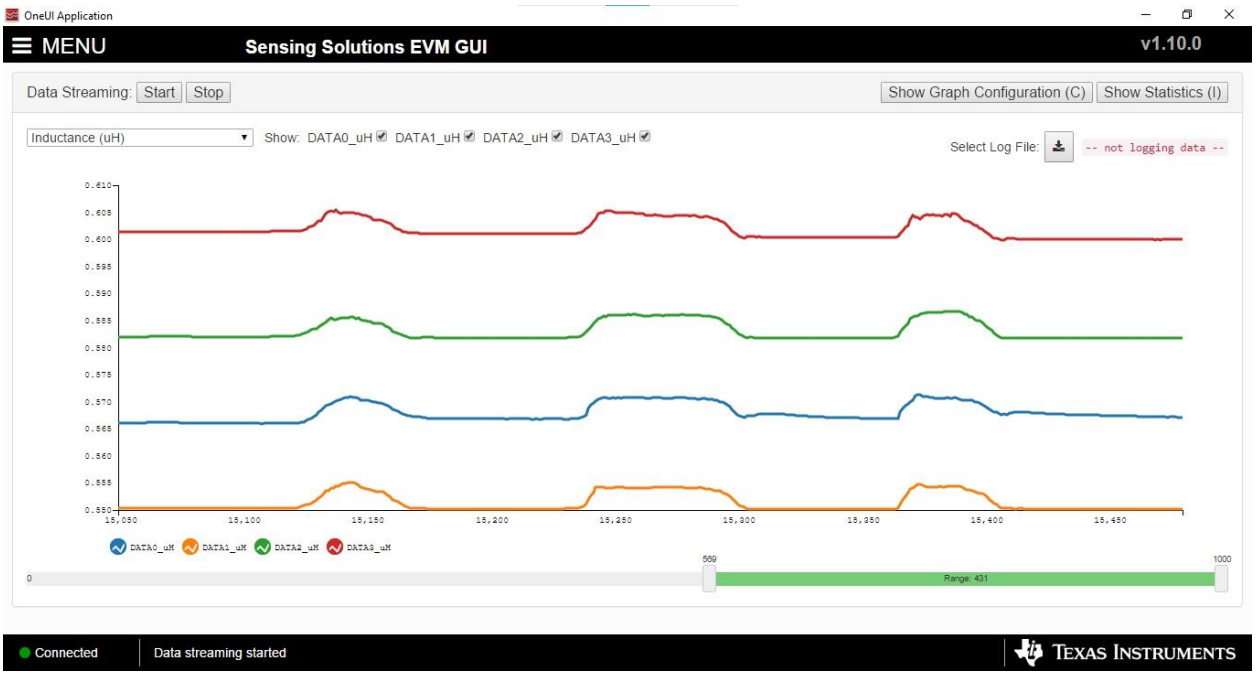

- For an understanding, a non-uniform normal force application by hand depicts changes in the inductance values of each coil due to changes in the frequency of the LC circuits as the magnetic coupling changes between the sensing coils and the sensing target.

Completion Certificate

It is certified that the thesis titled "***Development of a Three-Axis Inductive Force Sensor for Measuring Tool-Tissue Forces in Robotic Surgery.***" submitted by CMS ID. 0000317706, NS Muhammad Abdullah Khalid of MS-2019, Mechatronics Engineering is completed in all respects as per the requirements of Main Office, NUST (Exam branch).

Supervisor: _____

Dr. Muhammad Mubasher Saleem

Date: ____ Aug, 2022

THESIS ACCEPTANCE CERTIFICATE

Certified that final copy of MS/MPhil thesis written by Mr. Muhammad Abdullah Khalid, (Registration No. 00000317706), of NUST College of Electrical & Mechanical Engineering has been vetted by undersigned, found complete in all respects as per NUST Statues/Regulations, is within the similarity indices limit and is accepted as partial fulfillment for the award of MS/MPhil degree. It is further certified that necessary amendments as pointed out by GEC members of the scholar have also been incorporated in the said thesis.

Signature: _____

Name of Supervisor _____

Date: _____

Signature (HoD): _____

Date: _____

Signature (Dean/Principal): _____

Date: _____